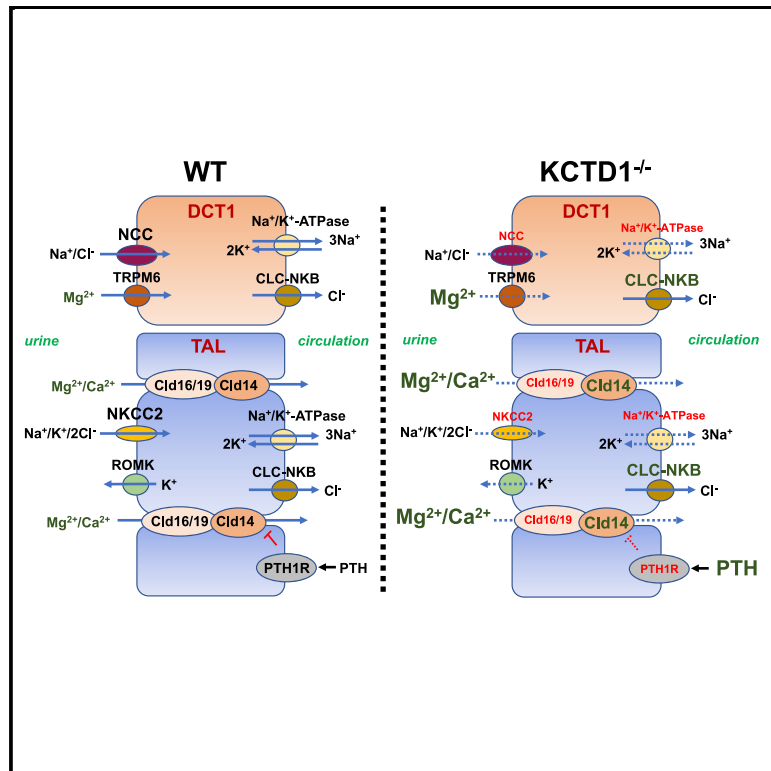


Magnesium and Calcium Homeostasis Depend on KCTD1 Function in the Distal Nephron

Graphical Abstract



Authors

Alexander G. Marneros

Correspondence

amarneros@mgh.harvard.edu

In Brief

Marneros shows that distal nephron defects from KCTD1 deficiency impair urinary transcellular Mg²⁺ reabsorption in distal convoluted tubules (DCTs) and paracellular Ca²⁺ and Mg²⁺ reabsorption in thick ascending limbs of Henle (TALs). Mice lacking KCTD1 develop hypomagnesemia and hypocalcemia, resulting in secondary hyperparathyroidism and consequently in progressive metabolic bone disease.

Highlights

- KCTD1 in early distal convoluted tubules regulates active urinary Mg²⁺ reabsorption
- EGF is not a major regulator of Mg²⁺ homeostasis
- Lack of KCTD1 in thick ascending limbs impairs paracellular Ca²⁺ and Mg²⁺ reabsorption
- These thick ascending limb defects cause hypocalcemia and hyperparathyroidism



Article

Magnesium and Calcium Homeostasis Depend on KCTD1 Function in the Distal Nephron

Alexander G. Mamerros^{1,2,3,*}¹Cutaneous Biology Research Center, Massachusetts General Hospital, Charlestown, MA 02129, USA²Department of Dermatology, Harvard Medical School, Boston, MA 02115, USA³Lead Contact*Correspondence: amameros@mg.harvard.edu<https://doi.org/10.1016/j.celrep.2020.108616>**SUMMARY**

Magnesium (Mg^{2+}) homeostasis depends on active transcellular Mg^{2+} reuptake from urine in distal convoluted tubules (DCTs) via the Mg^{2+} channel TRPM6, whose activity has been proposed to be regulated by EGF. Calcium (Ca^{2+}) homeostasis depends on paracellular reabsorption in the thick ascending limbs of Henle (TALs). KCTD1 promotes terminal differentiation of TALs/DCTs, but how its deficiency affects urinary Mg^{2+} and Ca^{2+} reabsorption is unknown. Here, this study shows that DCT1-specific KCTD1 inactivation leads to hypomagnesemia despite normal TRPM6 levels because of reduced levels of the sodium chloride co-transporter NCC, whereas Mg^{2+} homeostasis does not depend on EGF. Moreover, KCTD1 deficiency impairs paracellular urinary Ca^{2+} and Mg^{2+} reabsorption in TALs because of reduced NKCC2/claudin-16/-19 and increased claudin-14 expression, leading to hypocalcemia and consequently to secondary hyperparathyroidism and progressive metabolic bone disease. Thus, KCTD1 regulates urinary reabsorption of Mg^{2+} and Ca^{2+} by inducing expression of NCC in DCTs and NKCC2/claudin-16/-19 in TALs.

INTRODUCTION

The distal nephron of the kidney has a critical role for magnesium (Mg^{2+}) and calcium (Ca^{2+}) homeostasis by regulating the reabsorption of filtered Mg^{2+} and Ca^{2+} from urine. Mg^{2+} homeostasis depends largely on the rate of Mg^{2+} uptake by the intestine and by urinary Mg^{2+} excretion. Mechanisms of filtered Mg^{2+} reabsorption from urine in the kidney are, therefore, essential for tight regulation of Mg^{2+} serum levels and overall Mg^{2+} homeostasis. Most reabsorption of filtered Mg^{2+} in the kidney occurs via a paracellular mechanism in the proximal tubules (PTs) and the thick ascending limbs of Henle (TALs) (Mount, 2014). However, the distal convoluted tubule (DCT) is the primary site for active transcellular reabsorption of Mg^{2+} and accounts for ~10% of urinary Mg^{2+} uptake, which is mediated by the apical Mg^{2+} channel TRPM6 (Voets et al., 2004). This active transcellular Mg^{2+} uptake in the DCT is critical for the fine regulation of Mg^{2+} serum levels, and mutations in *TRPM6* lead to familial hypomagnesemia (Schlingmann et al., 2002; Walder et al., 2002). The DCT is separated into an early segment (DCT1), which transitions from the TAL, and a later segment (DCT2), which leads to the connecting tubule (CT). DCT cells are identified by their specific expression of the thiazide-sensitive apical Na^+Cl^- co-transporter NCC. DCT1 cells selectively express parvalbumin (Pvalb), whereas DCT2 cells express calbindin- D_{28K} (DCT1: NCC^+Pvalb^+ ; DCT2: $NCC^+Calbindin-D_{28K}^+$). Both parvalbumin and calbindin- D_{28K} are cytoplasmic Mg^{2+} and Ca^{2+} binding proteins, and >80% of Pvalb-binding sites are occupied by Mg^{2+} in DCT1 epithelial cells. TRPM6 is expressed in the entire DCT, albeit with higher

abundance in the DCT1. The activity of TRPM6 has been proposed to be regulated by the growth factor EGF, which is expressed in the kidney mainly by TAL and DCT cells. A C3209T missense mutation in *EGF*, which results in a P1070L amino acid change, was identified in a single, small family with isolated autosomal recessive hypomagnesemia (LOD score of only 2.66) (Groenestege et al., 2007). This C3209T variant is present only very rarely in the general population. However, the fact that this rare EGF variant has been linked to hypomagnesemia only in a single, small family raises the question as to the functional significance of EGF for controlling Mg^{2+} homeostasis. Immunolabeling detects EGF in the kidney mainly at the apical membranes of TALs and DCTs (Mamerros, 2020). Despite this apical localization of EGF *in vivo*, *in vitro* studies suggested that the P1070L amino acid change in EGF results in impaired basolateral sorting of pro-EGF and diminishes EGFR stimulation, which has been proposed to impair activation of the epithelial Mg^{2+} channel TRPM6 and lead to urinary Mg^{2+} wasting (Groenestege et al., 2007). Thus, whereas EGF may participate to some extent in the regulation of Mg^{2+} transport in DCTs, whether EGF is indeed a major magnesiotropic factor remains to be shown and the *in vivo* relevance of EGF for Mg^{2+} homeostasis requires further validation.

In contrast, a well-established cause for familial renal Mg^{2+} wasting is inactivating mutations in *SLC12A3*, encoding the gene for NCC, in patients with Gitelman syndrome, the most common form of familial hypomagnesemia (Simon et al., 1996c). NCC is found in the kidney in apical membranes of DCTs, and mutations in *SLC12A3* reduce Na^+ influx into the



cell, which is needed to maintain basolateral Na^+/K^+ -ATPase function, which establishes a low intracellular Na^+ concentration that promotes Na^+ entry apically and possibly Mg^{2+} exit at the basal side in DCT cells (Loffing et al., 2001). Thus, it has been proposed that loss of NCC impairs the electrolyte gradient required for transcellular Mg^{2+} transport in DCT cells, resulting in urinary Mg^{2+} wasting and hypomagnesemia in patients with Gitelman syndrome or in $\text{Slc12a3}^{-/-}$ mice (Schultheis et al., 1998; Simon et al., 1996c). Notably, Pvalb regulates NCC expression in DCT1s by modulating intracellular Ca^{2+} signaling, and Pvalb $^{-/-}$ mice have reduced renal NCC (Belge et al., 2007). Overall, the DCT1 is considered to be the main site for active transcellular Mg^{2+} transport in the kidney, is the only site of renal Pvalb expression, and is the nephron segment where TRPM6 and NCC have their highest expression (Xi et al., 2009).

The distal nephron is also a critical site for regulation of Ca^{2+} homeostasis. Ca^{2+} enters the tubular apparatus via glomerular filtration, and 98% of it is reabsorbed through either transcellular or paracellular mechanisms (Moor and Bonny, 2016). Most urinary Ca^{2+} is reabsorbed in the PTs (~65%) and TALs (~25%) through paracellular mechanisms, whereas only a relatively small fraction of urinary Ca^{2+} (~8%) is reabsorbed through transcellular mechanisms in the DCT2s and CTs (the collecting ducts [CDs] do not reabsorb Ca^{2+}) (Blaine et al., 2015).

A critical role for the transcriptional regulator KCTD1 has now been identified for the terminal differentiation and function of TAL and DCT epithelia (Marneros, 2020). KCTD1 is a BTB-domain-containing nuclear protein, whose *in vivo* functions were previously not known (Ding et al., 2008, 2009; Li et al., 2014; Marneros et al., 2013). This study found that the transcription factor AP-2 β is required for the formation of early-stage DCTs during nephrogenesis, whereas KCTD1 expression in the distal nephron is induced by AP-2 β and is required for the proper terminal differentiation of early-stage DCTs into mature, terminally differentiated DCTs (Marneros, 2020). Inactivation of KCTD1 in nephron progenitor cells (Six2Cre $^+$ KCTD1 $^{fl/fl}$ mice) impairs DCT and TAL function, resulting in a salt-losing tubulopathy and progressive renal failure, which is associated with diminished expression of the salt transporters NCC (in DCTs) and NKCC2 (in TALs) (Marneros, 2020). Notably, diminished activities of NCC and NKCC2 have been linked to similar clinical findings in patients with congenital salt-losing tubulopathies (Gitelman syndrome and Bartter syndrome) (Simon et al., 1996a, 1996c). The AP-2 β /KCTD1 axis is further demonstrated to be not only essential for the induction but also for the maintenance of the terminal differentiation state of TALs/DCTs in adults (Marneros, 2020). Although EGF expression in TALs/DCTs is found to be dependent on KCTD1, the terminal differentiation defect of TALs/DCTs in mice lacking KCTD1 occurs largely independent of EGF because EGF $^{-/-}$ mice do not phenocopy the renal abnormalities seen in KCTD1 $^{-/-}$ mice (Marneros, 2020).

Here, this study investigated whether KCTD1 deficiency impairs urinary Mg^{2+} and Ca^{2+} reabsorption in the kidney and affects overall Mg^{2+} and Ca^{2+} homeostasis. The findings show that, when KCTD1 is inactivated specifically in the DCT1 (in PvalbCre $^+$ KCTD1 $^{fl/fl}$ mice), hypomagnesemia and urinary Mg^{2+} wasting occur in association with diminished NCC expression, despite normal renal TRPM6 protein levels. Surprisingly, EGF

deficiency (in EGF $^{-/-}$ mice) does not result in hypomagnesemia, suggesting that EGF is not a major regulator of Mg^{2+} homeostasis. Thus, KCTD1-mediated terminal differentiation of DCT1s is required for high-level NCC expression in this nephron segment and is critical for its ability to maintain transcellular Mg^{2+} transport, whereas EGF is not essential for that process. Furthermore, KCTD1 deficiency in the kidney was found to lead to functional TAL defects that impair the ability of this nephron segment to reabsorb Ca^{2+} from urine, resulting in urinary Ca^{2+} wasting, which leads to hypocalcemia, secondary hyperparathyroidism, and consequently, progressive metabolic bone disease. Mechanistically, the findings link the Ca^{2+} transport defect to impaired expression of key regulators of paracellular Ca^{2+} transport in the TAL as a consequence of KCTD1 deficiency: the TAL-specific loop diuretic-sensitive $\text{Na}^+/\text{K}^+/\text{2Cl}^-$ co-transporter NKCC2 is critical for the ability of TALs to concentrate urine and for maintaining a lumen-positive electrical gradient that drives paracellular Ca^{2+} and Mg^{2+} reabsorption in TALs (Mount, 2014), and constitutive or induced inactivation of KCTD1 resulted in diminished NKCC2 levels in TALs. This reduction in NKCC2 was associated with an impaired ability of the kidney to reabsorb urinary Ca^{2+} in TALs, resulting in urinary Ca^{2+} wasting. Hypercalciuria was linked not only to NKCC2 loss but also to reduced expression of PTH1R and claudin-16/19 and increased expression of claudin-14, which are all important regulators of paracellular Ca^{2+} and Mg^{2+} reabsorption in TALs. Thus, KCTD1 function in the distal nephron is required for renal regulation of Mg^{2+} and Ca^{2+} homeostasis.

RESULTS

Inactivation of AP-2 β or KCTD1 in DCT1s Results in Hypomagnesemia

PvalbCre $^+$ mice allow for selective inactivation of genes in the DCT1s (Figure 1A). Inactivation of KCTD1 or AP-2 β only in DCT1s (PvalbCre $^+$ KCTD1 $^{fl/fl}$ mice and PvalbCre $^+$ TFAP2B $^{fl/fl}$ mice) did not impair overall kidney function (Figures S1A and S1B). However, already young (2-month-old) PvalbCre $^+$ KCTD1 $^{fl/fl}$ and PvalbCre $^+$ TFAP2B $^{fl/fl}$ mice had significant hypomagnesemia, which was maintained with age (Figures 1B and S1B). Despite normal urine production, Mg^{2+} urine concentration was increased in PvalbCre $^+$ KCTD1 $^{fl/fl}$ mice (Figures 1C and S1A). Similarly, inducible inactivation of KCTD1 in adults also resulted in hypomagnesemia (Figure 1D). In contrast, inactivation of KCTD1 in the intestines (VilCre $^+$ KCTD1 $^{fl/fl}$ mice) or the CTs/CDs (Aqp2Cre $^+$ KCTD1 $^{fl/fl}$ mice) did not affect serum Mg^{2+} levels (Figure 1D). The hypomagnesemia in both PvalbCre $^+$ KCTD1 $^{fl/fl}$ mice and PvalbCre $^+$ TFAP2B $^{fl/fl}$ mice was associated with reduced renal NCC protein levels, whereas TRPM6 protein levels were not reduced (Figure 1E). Similarly, expression of TRPM6 was not reduced in Six2Cre $^+$ KCTD1 $^{fl/fl}$ mice (lacking KCTD1 in the entire nephron, except the CDs), which had strongly decreased Slc12a3 (NCC) transcript levels in their kidneys at 2 months of age (Figure 1F) as shown previously (Marneros, 2020). Analysis of RNA sequencing (RNA-seq) data from kidneys of P8 Six2Cre $^+$ KCTD1 $^{fl/fl}$ mice or of mice with inducible inactivation of AP-2 β in the adult showed that, among genes that have been implicated in the regulation of renal Mg^{2+} transport, only

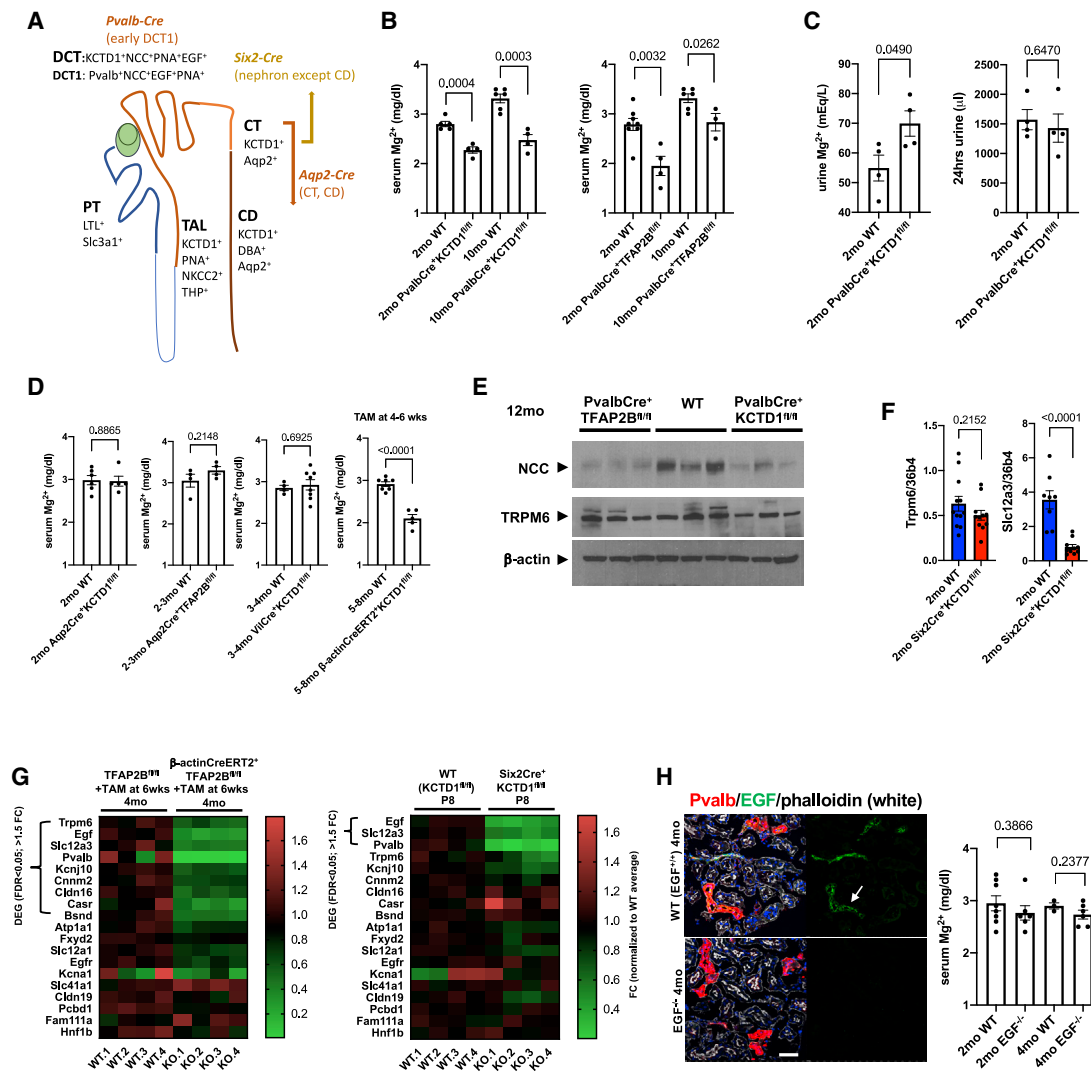


Figure 1. Inactivation of AP-2β or KCTD1 in DCT1s Results in Hypomagnesemia Independently of EGF

(A) Conditional gene-targeting strategy depicted in the schematic. *PvalbCre* leads to Cre-mediated recombination of floxed alleles specifically in the DCT1, whereas *Aqp2Cre* mice target CTs/CDs. *Six2Cre* mice target the entire nephron, except the CDs. KCTD1 is expressed in the distal nephron (TALs, DCTs, CTs, and CDs). DBA (dolichos biflorus agglutinin) lectin marks CTs/CDs, PNA (peanut agglutinin) lectin marks distal nephron epithelium (discontinuous epithelial staining in TALs, DCTs, and CTs/CDs; continuous labeling of PTs), and LTL (lotus tetragonolobus lectin) marks PTs. *Slc3a1* is expressed in PTs, *NKCC2* and *THP* in TALs, *NCC* in DCTs, *Pvalb* in DCT1s, and *Aqp2* in CTs/CDs. *EGF* is detected in DCTs and TALs.

(B) Serum Mg²⁺ levels (in mg/dL) in groups of 2- or 10-month-old *PvalbCre*⁺KCTD1^{fl/fl} or *PvalbCre*⁺TFAP2B^{fl/fl} mice and their Cre-negative control littermates (WT).

(C) Urine Mg²⁺ concentrations (in mEq/L) are increased in 2-month-old *PvalbCre*⁺KCTD1^{fl/fl} mice when compared with their controls, despite normal 24-h urine production in the same mice.

(D) Tamoxifen-induced inactivation of KCTD1 at 4–6 weeks of age results in hypomagnesemia when assessed at 5–8 months of age (*β-actinCreERT2*⁺KCTD1^{fl/fl} mice + TAM). Inactivation of KCTD1 in intestines (*VilCre*⁺KCTD1^{fl/fl} mice) or of KCTD1 or AP-2β in CTs/CDs (*Aqp2Cre*⁺KCTD1^{fl/fl} or *Aqp2Cre*⁺TFAP2B^{fl/fl} mice) does not affect serum Mg²⁺ levels.

(E) Kidneys of adult *PvalbCre*⁺KCTD1^{fl/fl} or *PvalbCre*⁺TFAP2B^{fl/fl} mice show reduced protein levels of NCC but not of TRPM6; 12-month-old mice. β-actin as the loading control.

(F) Semiquantitative RT-PCR for *Trpm6* and *Slc12a3* in whole kidneys of 2-month-old *Six2Cre*⁺KCTD1^{fl/fl} mice and their littermate controls.

(G) Heatmaps show expression levels of genes implicated in the regulation of Mg²⁺ homeostasis in the kidney. RNA-seq data from kidneys of mice with induced inactivation of AP-2β in the adult (4-month-old *β-actinCreERT2*⁺TFAP2B^{fl/fl} mice treated with TAM at 6 weeks of age) and their Cre⁻ controls (left) or from kidneys of P8 *Six2Cre*⁺KCTD1^{fl/fl} mice and their Cre⁻ control littermates (Marneros, 2020). Differentially expressed genes (DEGs) (>1.5-fold change [FC] in expression; false discovery rate [FDR] < 0.05) are indicated. In both mutant groups, the DCT-expressed genes *EGF*, *Slc12a3*, and *Pvalb* are significantly downregulated. Scale shows FC normalized to the control group average.

(H) *EGF* (arrow) is detected in *Pvalb*⁺ DCT1s at the apical cell membrane (*EGF* in green, *Pvalb* in red). No *EGF* is detected in kidneys of *EGF*^{-/-} mice. Scale bar, 50 μm. DAPI stains nuclei blue. Mg²⁺ serum levels are not significantly reduced in *EGF*^{-/-} mice compared with their WT littermates at 2 or 4 months of age. Graphs represent data as means ± SEM. Semiquantitative RT-PCRs performed in triplicate. p values are shown (two-tailed, unpaired t test). Related to Figure S1.

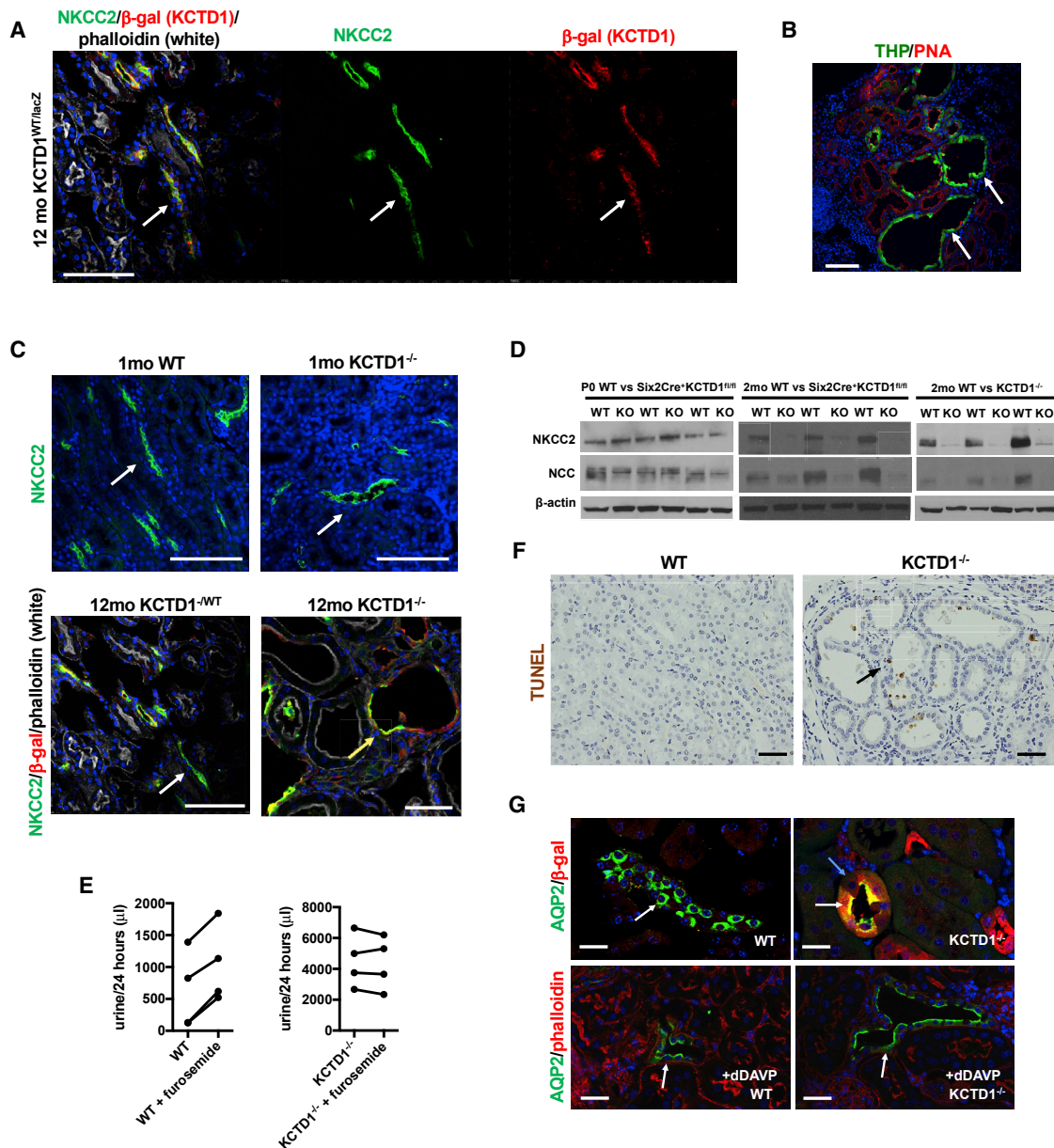


Figure 2. Lack of KCTD1 Leads to Progressive TAL Defects

(A) KCTD1 is expressed in TALs (arrows); β -galactosidase (red) in KCTD1^{WT/lacZ} mice is observed in NKCC2⁺ TALs (green); 12-month-old KCTD1^{WT/lacZ} mouse. Scale bar, 50 μ m.

(B) THP (green, arrows) marks TALs, which are dilated in aged KCTD1^{-/-} mice (8-month-old). Scale bar, 50 μ m.

(C) Top: mild dilatation of NKCC2⁺ TALs (green, white arrows) is observed in 1-month-old KCTD1^{-/-} mice. Scale bars, 100 μ m. Bottom: 12-month-old KCTD1^{-/-} mice, expressing β -galactosidase (red) from the endogenous KCTD1 locus, show extensive TAL dilatations with discontinuous and irregular expression of NKCC2 (green; yellow arrow); 12-month-old KCTD1^{-WT} mice show normal NKCC2 labeling in normal-appearing β -gal⁺ TALs (white arrow). Scale bars, 50 μ m.

(D) Western blot with kidney lysates for NKCC2 and NCC. Kidneys of Six2Cre⁺KCTD1^{fl/fl} mice at birth (P0) show no major reduction in NKCC2 and NCC protein levels. In contrast, 2-month-old Six2Cre⁺KCTD1^{fl/fl} or KCTD1^{-/-} mice show a strong decrease in NKCC2 and NCC protein levels compared with their control littermates. β -actin as loading control.

(E) WT mice increase their 24-h urine production when treated with the NKCC2 inhibitor furosemide. Diminished levels of NKCC2 in KCTD1^{-/-} mice correlate with a lack of a response to furosemide; 2-month-old mice (n = 4).

(F) Few apoptotic cells (TUNEL⁺, arrow) in dilated distal nephron tubules in 9-month-old KCTD1^{-/-} mice are being extruded into their lumina. No apoptotic cells in 9-month-old WT littermates. Scale bar, 50 μ m.

(legend continued on next page)

Slc12a3, EGF, and Pvalb were downregulated greater 1.5-fold in both mutants (Figure 1G) (Marneros, 2020). Collectively, these findings demonstrate that AP-2 β /KCTD1 function in DCT1s is critical for NCC expression and for urinary Mg²⁺ reuptake in this nephron segment.

Role of EGF for Urinary Mg²⁺ Reabsorption

EGF expression occurs in TALs and DCTs with the induction of their terminal differentiation (after P3) (Marneros, 2020). Immunolabeling shows mainly an apical membrane localization of EGF in TALs and DCTs (Figure 1H) (Marneros, 2020). Adult Six2-Cre⁺KCTD1^{fl/fl} or KCTD1^{-/-} mice show a complete absence of EGF protein in their TALs and DCTs (Figure 1H) (Marneros, 2020). However, lack of EGF in DCTs due to KCTD1 deficiency is only a marker of the terminal differentiation defect and is not responsible for the functional and morphological DCT abnormalities that occur due to lack of KCTD1 because EGF^{-/-} mice did not develop those DCT abnormalities when examined at 6 weeks of age when KCTD1^{-/-} mice had already developed morphological DCT abnormalities (Marneros, 2020). Even at 4 months old, DCT1s had a normal morphological appearance in EGF^{-/-} mice (Figure 1H). To test the physiological relevance of EGF for the ability of DCTs to reabsorb urinary Mg²⁺, it was assessed whether EGF^{-/-} mice develop hypomagnesemia. Serum Mg²⁺ levels in 2- or 4-month-old EGF^{-/-} mice were not significantly reduced (Figure 1H). This demonstrates that if EGF participates in the regulation of Mg²⁺ transport in DCTs, it does not have a major rate-limiting role. Thus, hypomagnesemia that occurs because of the lack of KCTD1 in DCT1s is associated with reduced levels of NCC and occurs largely independently of EGF regulation.

Lack of KCTD1 Impairs TAL/DCT Function

Consistent with single-cell RNA-seq data showing that KCTD1 is expressed in the kidney, specifically in the distal nephron epithelium (Lindström et al., 2018; Park et al., 2018; Ransick et al., 2019), strong reporter gene expression (β -galactosidase) was observed in KCTD1 reporter mice only in the distal nephron epithelium, including the TALs (NKCC2 serves as a specific marker for TALs) (Figure 2A) and DCTs, whereas no KCTD1 expression was observed in glomeruli, PTs, or stromal cells of the kidney (Figure 1A) (Marneros, 2020). Immunolabeling for the TAL markers NKCC2 or THP (Tamm-Horsfall protein) demonstrated that TALs lacking KCTD1 showed a progressive age-dependent dilatation associated with irregular and discontinuous NKCC2 labeling (Figures 2B and 2C).

Kidneys of newborn Six2Cre⁺KCTD1^{fl/fl} mice (P0) showed no major reduction in NKCC2 and NCC protein levels (Figure 2D), demonstrating that lack of KCTD1 does not prevent the formation of TALs and DCTs during nephrogenesis. However, the increase in NKCC2 and NCC levels that can normally be observed in wild-type (WT) mice with their postnatal terminal differentiation was not seen in mice lacking KCTD1 (Figure 2D). Thus, KCTD1 is

required for high-level expression of NKCC2 and NCC in the adult TALs and DCTs, respectively. Treatment of WT mice with the NKCC2 inhibitor and loop diuretic furosemide leads to reduced salt reabsorption in TALs and causes increased urine production, whereas it could not further increase the already-much-increased urine output in KCTD1^{-/-} mice (Figure 2E), consistent with a lack of NKCC2 function.

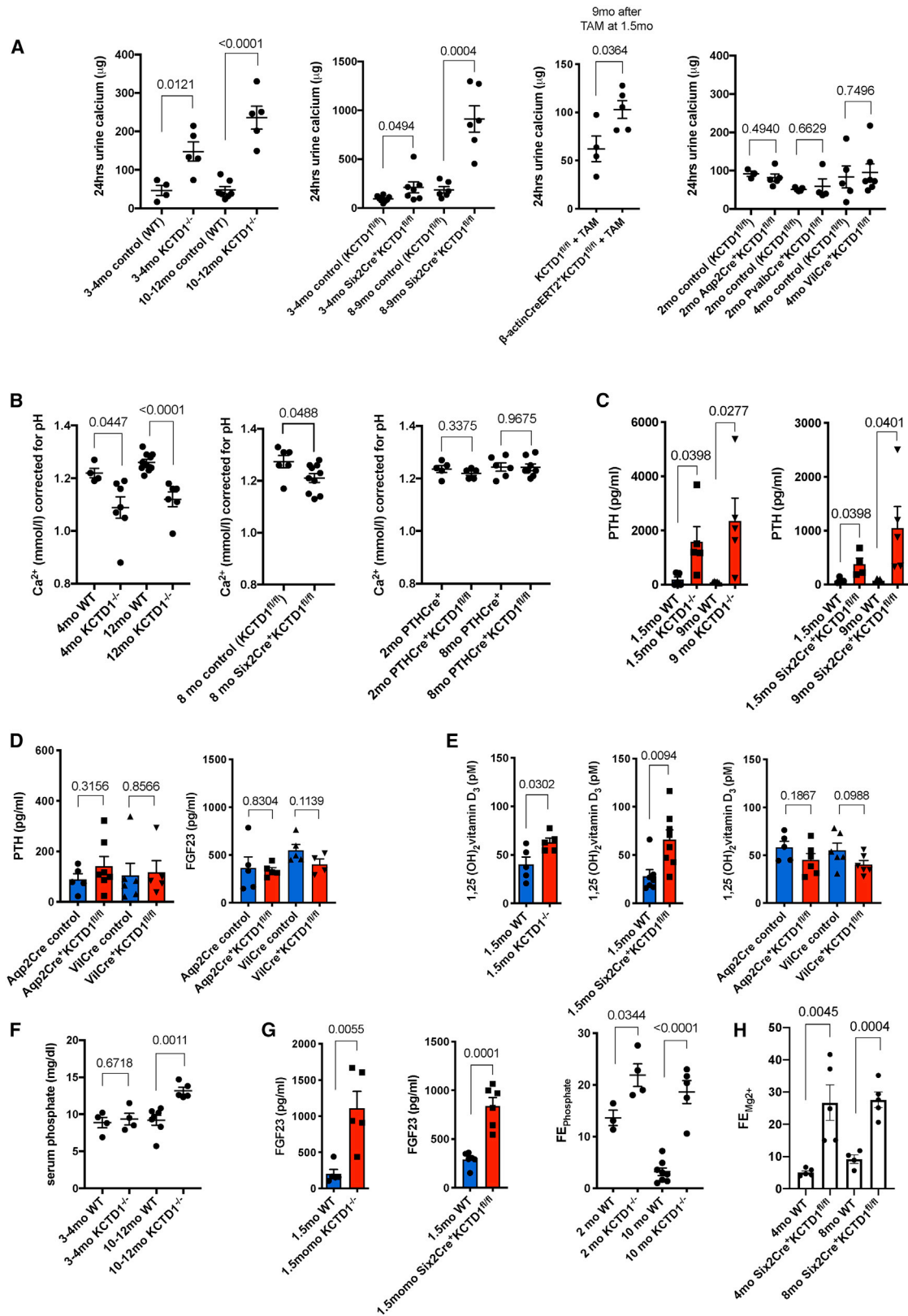
The observation of reduced and irregular NKCC2 immunolabeling in dilated TALs of adult KCTD1^{-/-} mice suggests that the low levels of NKCC2 protein in whole-kidney lysates of these mice are likely explained by a TAL terminal-differentiation defect and not by postnatal degeneration of TAL segments. This is also supported by the lack of significant apoptosis in the distal nephron epithelia even in aged KCTD1^{-/-} kidneys (Figure 2F). Only shedding of few apoptotic cells into the tubular lumen of distal nephron epithelia was observed but no frank apoptotic degeneration of nephron segments (Figure 2F). PTs and glomeruli, which do not express KCTD1 (β -galactosidase⁻ in KCTD1^{-/-} mice), had a normal morphological appearance in young adult KCTD1^{-/-} mice that only showed dilatation in distal nephron segments that normally express KCTD1 (β -galactosidase⁺) (Marneros, 2020). Moreover, no abnormalities were observed in the CDs of KCTD1^{-/-} mice. This is consistent with the observation that inactivation of KCTD1 in principle cells of CTs/CDs (which are the cell types that express KCTD1 in these segments) did not result in renal abnormalities (Aqp2-Cre⁺KCTD1^{fl/fl} mice) (Figure S1A).

The increased urinary water loss owing to the TAL/DCT defects in mice lacking KCTD1 evoked counterregulatory mechanisms in the CTs/CDs to reduce polyuria. Normally, vasopressin is released in response to water loss, which induces membrane trafficking of the water channel AQP2 from intracytoplasmic endosomes to the luminal epithelial membranes of CTs/CDs to stimulate transepithelial water transport as a counterregulatory mechanism to prevent excessive urinary water loss. KCTD1 deficiency did not prevent that function of CDs, and AQP2 was found in mice lacking KCTD1 at the luminal membrane in the CTs/CDs, whereas it was mostly cytoplasmic in control littermates (Figure 2G). Although the luminal membrane localization of AQP2 suggests that this counterregulatory mechanism is active in the CDs of KCTD1^{-/-} mice, it is not sufficient to prevent the polyuria that develops because of the TAL/DCT abnormalities. Collectively, these findings demonstrate that the lack of KCTD1 impairs TAL/DCT function and leads to a reduced ability of the kidney to concentrate urine.

KCTD1 Deficiency Causes Decreased Urinary Ca²⁺ Reabsorption That Leads to Hypocalcemia

Because TALs have important functions for both urinary Ca²⁺ and Mg²⁺ reabsorption, which are dependent on proper NKCC2 activity to maintain a lumen-positive electrical gradient that drives paracellular Ca²⁺ and Mg²⁺ reabsorption in the TAL, it was investigated whether TAL defects in mice lacking

(G) AQP2 is localized at the apical luminal membrane in β -gal⁺-expressing CTs/CDs of KCTD1^{-/-} mice even without administration of desmopressin (dDAVP; with similar effects like vasopressin in CTs/CDs), whereas AQP2 is localized in the cytoplasm in WT littermates without dDAVP administration and becomes only apically localized when treated with dDAVP; 4-month-old mice are shown. Scale bars, 20 μ m. DAPI stains nuclei blue.



(legend on next page)

KCTD1 also impaired urinary Ca^{2+} reabsorption. Indeed, both KCTD1^{-/-} and Six2Cre⁺KCTD1^{fl/fl} mice developed severe progressive urinary Ca^{2+} loss: calcium mass in 24-h urine collections was increased already in young adult KCTD1^{-/-} and Six2-Cre⁺KCTD1^{fl/fl} mice and further increased with age (Figure 3A). Inducible inactivation of KCTD1 in the adult leads to increased urinary Ca^{2+} loss as well (Figure 3A). Thus, diminished levels of NKCC2 from KCTD1 deficiency are associated with significant hypercalciuria, similar to that observed in mice and humans that have NKCC2 mutations (Kemter et al., 2010; Simon et al., 1996a). Urinary Ca^{2+} loss in KCTD1^{-/-} and Six2Cre⁺KCTD1^{fl/fl} mice was accompanied by chronic hypocalcemia with reduced levels of ionized calcium (Ca^{2+}) serum levels (Figure 3B). In contrast, lack of KCTD1 in CTs/CDs (in Aqp2Cre⁺KCTD1^{fl/fl} mice), in DCT1s (in PvalbCre⁺KCTD1^{fl/fl} mice), or in the intestinal tract (in VilCre⁺KCTD1^{fl/fl} mice) did not result in urinary Ca^{2+} loss (Figure 3A). Because (1) KCTD1 is not expressed in glomeruli and PTs and because (2) conditional inactivation of KCTD1 specifically in DCT1s, CTs, and CD does not result in urinary Ca^{2+} wasting, and whereas (3) even young adult Six2Cre⁺KCTD1^{fl/fl} mice that show no morphological abnormalities of the PTs or glomeruli at that age develop hypercalciuria, a primary defect in DCT2s and/or TALs of these mice is most likely responsible for the observed reabsorption defect of filtered Ca^{2+} in their kidney.

KCTD1 is not only expressed in the distal nephron epithelium but also in parathyroid glands (PTGs), organs that regulate serum calcium levels via secretion of parathyroid hormone (PTH) (Figure S2A). To ensure that the observed hypocalcemia in Six2-Cre⁺KCTD1^{fl/fl} mice is explained by the lack of KCTD1 in the kidney and not through potential inactivation of KCTD1 in PTGs through unexpected Six2Cre⁺ activity in PTGs, it was confirmed that the Six2Cre⁺ strain targeted floxed alleles in the nephron (except the CD) but not in PTGs by crossing Six2Cre⁺ mice with an EYFP-reporter strain (Figure S2B). In addition, inactivation of KCTD1 in PTGs in PTHCre⁺KCTD1^{fl/fl} mice did not affect ionized Ca^{2+} serum levels (Figures 3B and S2C) (Kobayashi et al., 2008; Libutti et al., 2003). Thus, the sustained hypocalcemia in

KCTD1^{-/-} and Six2Cre⁺KCTD1^{fl/fl} mice is explained by the lack of KCTD1 in their kidneys and not their PTGs.

Secondary Hyperparathyroidism due to Hypocalcemia in KCTD1^{-/-} Mice

Hypocalcemia stimulates PTGs to secrete PTH to counter low serum calcium levels by several mechanisms: it reduces urinary Ca^{2+} excretion in the kidney, it induces 1,25(OH)₂ vitamin D₃ production in the kidney to increase dietary calcium absorption in the gastrointestinal tract, it enhances fractional excretion of phosphate, and it targets the bone to increase efflux of calcium and phosphate (Quarles, 2008). Indeed, the sustained urinary Ca^{2+} loss and the hypocalcemia in mice lacking KCTD1 were associated with secondary hyperparathyroidism: KCTD1^{-/-} mice and Six2Cre⁺KCTD1^{fl/fl} mice showed a strong increase in serum PTH levels when examined at 1.5 or 9 months of age (Figure 3C). However, the secondary hyperparathyroidism in KCTD1^{-/-} mice and Six2Cre⁺KCTD1^{fl/fl} mice was not sufficient to compensate for the low serum calcium that occurred due to a substantial urinary Ca^{2+} loss in those mice. In contrast, PTH serum levels were normal in Aqp2Cre⁺KCTD1^{fl/fl} or Vil-Cre⁺KCTD1^{fl/fl} mice that had no increased urinary Ca^{2+} loss (Figure 3D). The reduced serum Ca^{2+} levels and the increased PTH in KCTD1^{-/-} and Six2Cre⁺KCTD1^{fl/fl} mice were associated with an increase in 1,25(OH)₂ vitamin D₃ serum levels (Figure 3E).

High PTH serum levels are often found early in the disease course of chronic kidney disease (CKD), whereas increased phosphate serum levels are often seen in late-stage CKD (Martin and González, 2007). Resembling these observations in human CKD, increases in serum PTH occurred early in KCTD1^{-/-} and Six2Cre⁺KCTD1^{fl/fl} mice, whereas serum phosphate levels were increased only late in the disease course in aged, but not in young, KCTD1-deficient mice (Figure 3F).

The phosphaturic hormone FGF23 is increased early in the disease course in CKD and produced by bone to counter increased serum phosphate levels by stimulating fractional excretion of phosphate and inhibiting 1 α -hydroxylase activity in the kidney (Quarles, 2008). Mice lacking KCTD1 also had highly

Figure 3. KCTD1 Deficiency Leads to Urinary Ca^{2+} Wasting, Hypocalcemia, and Chronic Secondary Hyperparathyroidism

(A) 24-h urine collections demonstrate that KCTD1^{-/-} and Six2Cre⁺KCTD1^{fl/fl} mice have significantly increased urinary calcium loss compared with their littermate controls. This urinary calcium wasting increases with deterioration of kidney function with progressive age. Inducible inactivation of KCTD1 in the adult at 6-weeks of age also results in urinary calcium wasting. In contrast, lack of KCTD1 in principle cells of the CTs/CDs (Aqp2Cre⁺KCTD1^{fl/fl} mice), in DCT1s (PvalbCre⁺KCTD1^{fl/fl} mice), or in the intestines (VilCre⁺KCTD1^{fl/fl} mice) does not affect urinary calcium reabsorption. 24-h urine calcium mass in micrograms is indicated.

(B) Free ionized serum calcium (Ca^{2+}) corrected for pH is decreased in both 4-month-old adult and 12-month-old aged KCTD1^{-/-} mice when compared with littermate controls. Aged Six2Cre⁺KCTD1^{fl/fl} mice (8-month-old mice) also show a decrease in serum Ca^{2+} levels. In contrast, PTHCre⁺KCTD1^{fl/fl} mice have normal serum Ca^{2+} levels. Ca^{2+} in micromoles per liter.

(C) Serum active PTH levels are already highly increased in 1.5-month-old KCTD1^{-/-} and Six2Cre⁺KCTD1^{fl/fl} mice and are further increased in 9-month-old mutants. PTH concentration in picograms per milliliter.

(D) Aqp2Cre⁺KCTD1^{fl/fl} or VilCre⁺KCTD1^{fl/fl} mice have normal PTH and FGF23 serum levels. 3–4-month-old mice. PTH and FGF23 concentrations in picograms per milliliter.

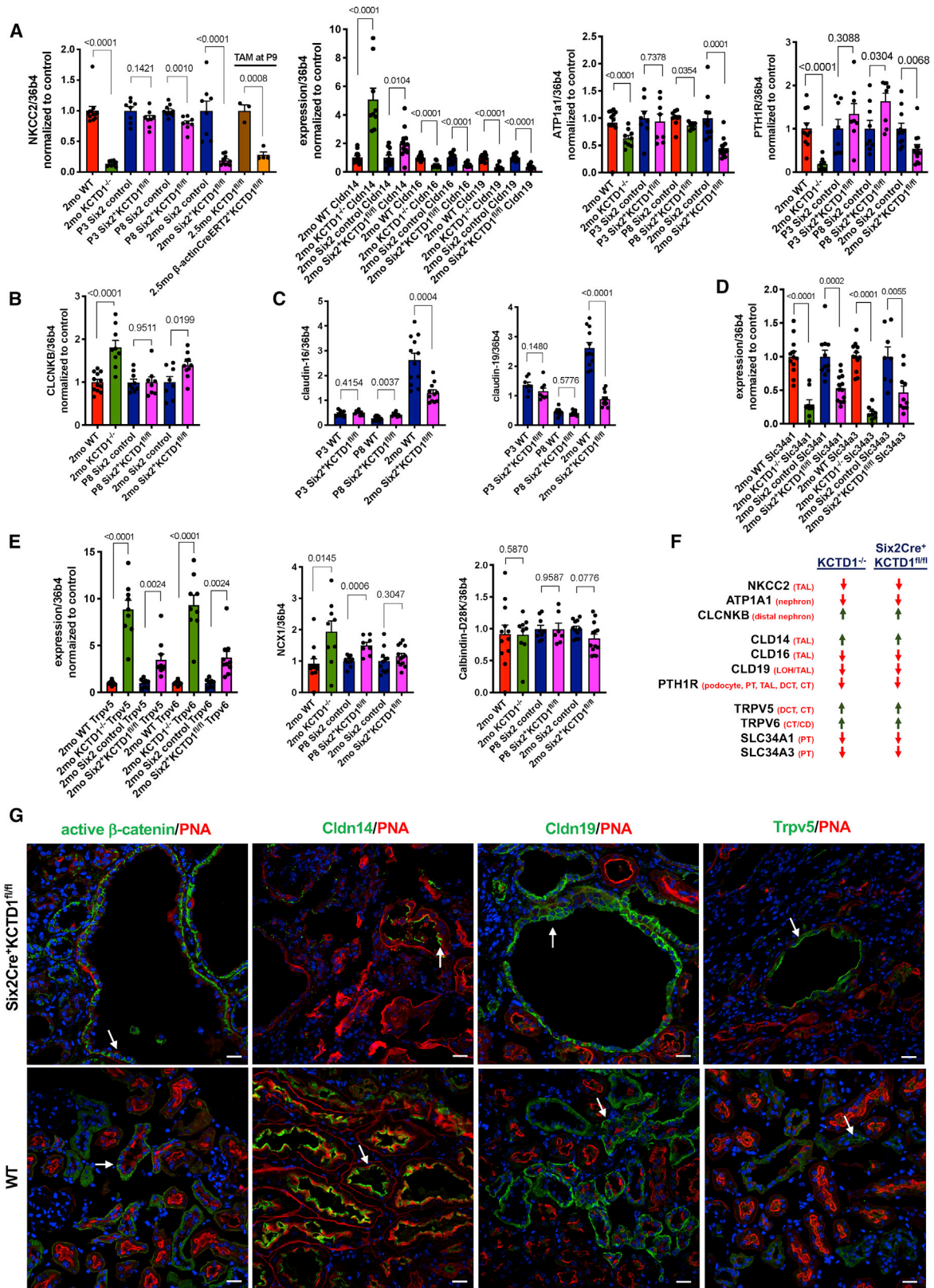
(E) Serum levels of 1,25(OH)₂ vitamin D₃ are moderately increased in 1.5-month-old KCTD1^{-/-} and Six2Cre⁺KCTD1^{fl/fl} mice compared with their littermate controls, whereas no increase is observed in 3–4-month-old Aqp2Cre⁺KCTD1^{fl/fl} or VilCre⁺KCTD1^{fl/fl} mice. Concentrations in picomolar.

(F) An increase in serum phosphate levels is detected only in aged (10–12-month-old) but not in young (3–4-month-old) KCTD1^{-/-} mice. Shown in milligrams per deciliter.

(G) FGF23 serum levels (in pg/mL) are highly increased in 1.5-month-old KCTD1^{-/-} and Six2Cre⁺KCTD1^{fl/fl} mice compared with their littermates. This correlates with increased fractional excretion of phosphate ($\text{FE}_{\text{phosphate}}$) in both 2- and 10-month-old KCTD1^{-/-} mice.

(H) Increased fractional excretion of Mg^{2+} ($\text{FE}_{\text{Mg}^{2+}}$) in both 4- and 8-month-old Six2Cre⁺KCTD1^{fl/fl} mice.

Graphs represent data as means \pm SEM. p values are shown (two-tailed, unpaired t test). Related to Figure S2.



(legend on next page)

increased FGF23 serum levels and increased fractional phosphate excretion already at a young age (Figure 3G). That high increase in FGF23 already in young mice lacking KCTD1 is likely also explained in part by impaired renal function with increased blood urea nitrogen (BUN), which was already observed at that age (Figure S1A). In contrast, *Aqp2Cre⁺KCTD1^{fl/fl}* and *Vil-Cre⁺KCTD1^{fl/fl}* mice, which had normal urinary Ca^{2+} and serum PTH levels, also had normal FGF23 serum levels (Figure 3D). Notably, the hypercalciuria in mice lacking KCTD1 in the kidney was accompanied by increased fractional excretion of Mg^{2+} in those mice (Figure 3H).

TAL Defects in Mice Lacking KCTD1 Impair Paracellular Ca^{2+} and Mg^{2+} Reabsorption due to Diminished NKCC2 and Claudin-16/-19 and Increased Claudin-14 Expression

A significant portion of filtered Mg^{2+} and Ca^{2+} is transported back into the circulation via a paracellular pathway in the TALs. Thus, urinary Mg^{2+} wasting as a consequence of KCTD1 deficiency in the kidney likely occurs not only due to impaired transcellular Mg^{2+} transport in DCT1s but also as a consequence of reduced paracellular transport in partly dysfunctional TALs. In contrast, the observations in the various conditional mutant mice with inactivation of KCTD1 in distinct nephron segments combined with the distal nephron-specific expression pattern of KCTD1 suggest that the impaired urinary Ca^{2+} reabsorption in KCTD1 mutant mice occurs because of defects in DCT2s and/or TALs because inactivation of KCTD1 in DCT1s or CTs/CDs did not affect urinary Ca^{2+} levels. To further test whether functional defects in DCTs or TALs explain the urinary Ca^{2+} wasting in KCTD1 mutant mice and to gain insights into the pathomechanisms involved, it was assessed how KCTD1 deficiency affects the expression of DCT- and TAL-specific genes that have key roles in Ca^{2+} transport processes in these segments.

The K^+ channel ROMK in the TAL ensures adequate luminal K^+ levels for continuous $\text{Na}^+ - \text{K}^+ - 2\text{Cl}^-$ uptake by NKCC2 and generates a lumen-positive electrical gradient that drives paracellular Ca^{2+} and Mg^{2+} reabsorption in the TAL (Mount, 2014). The

$\text{Na}^+ - \text{K}^+$ ATPase is critical for Na^+ exit at the basolateral membrane and generates a Na^+ gradient that drives apical Na^+ , K^+ , and Cl^- entry into TAL cells via NKCC2. ATP1A1 (the $\alpha 1$ subunit of the $\text{Na}^+ - \text{K}^+$ ATPase) is broadly expressed in the nephron but shows the highest expression levels in TALs/DCTs/CTs (Ransick et al., 2019). PTH/PTH1R signaling stimulates urinary Ca^{2+} reabsorption in the TAL indirectly by promoting NKCC2-mediated salt reabsorption and directly by suppressing the expression of claudin-14 that inhibits Ca^{2+} reabsorption in the TAL (Sato et al., 2017). PTH1R is also expressed in podocytes and PTs (Ransick et al., 2019). Claudins-16 and -19 are critical for the cation selectivity of TAL tight junctions and promote Ca^{2+} and Mg^{2+} paracellular reabsorption in the TAL, whereas claudin-14 has the opposite effect. The predominant expression of claudin-16 and claudin-14 in the nephron occurs in TALs (Ransick et al., 2019).

Semiquantitative RT-PCR of kidneys of 2-month-old *KCTD1^{-/-}* and *Six2Cre⁺KCTD1^{fl/fl}* mice (compared with their control littermates) showed that the increased urinary Ca^{2+} and Mg^{2+} loss in those mutant mice was associated with strongly reduced renal expression of NKCC2, ATP1A1, PTH1R, claudin-16, and claudin-19 but increased expression of claudin-14 (Figure 4A). The diminished NKCC2 transcript levels are also consistent with the observation of reduced NKCC2 protein levels in kidneys of *KCTD1^{-/-}* and *Six2Cre⁺KCTD1^{fl/fl}* mice (Figure 2D) (Marnaros, 2020). The increase in expression of claudin-14 demonstrates that the observed expression changes are not due to a complete dedifferentiation of TALs and that, despite KCTD1 deficiency, TALs maintain, at least in part, the ability to increase expression of TAL genes (such as claudin-14). Similarly, expression of the distal nephron basolateral chloride channel *CLCNKB* was also increased in the kidneys of mice lacking KCTD1 (Figure 4B). Overall, these findings suggest that reduced paracellular reabsorption of filtered Ca^{2+} and Mg^{2+} in the TAL occurs because of reduced NKCC2/ATP1A1/PTH1R/claudin-16/19 and increased claudin-14 expression (Figure 4A).

Assessing the expression of claudin-16 and -19 in *Six2-Cre⁺KCTD1^{fl/fl}* mice at different time points postnatally shows

Figure 4. Diminished Expression of NKCC2/ATP1a1/PTH1R/Claudin-16/-19 and Increased Expression of Claudin-14 Are Associated with the Urinary Ca^{2+} Reabsorption Defect in TALs Lacking KCTD1

- (A) Semiquantitative RT-PCR in kidneys of 2-month-old *KCTD1^{-/-}* and *Six2Cre⁺KCTD1^{fl/fl}* mice shows a significant decrease in NKCC2 (encoded by *Slc12a1*) transcripts compared with their littermate controls. P3 *Six2Cre⁺KCTD1^{fl/fl}* mice show normal NKCC2 levels, and P8 *Six2Cre⁺KCTD1^{fl/fl}* mice show a modest reduction in NKCC2 expression. Inducible inactivation of KCTD1 with TAM at P9 in β -actinCreERT2⁺*KCTD1^{fl/fl}* mice results in strong reduction of NKCC2 expression in the kidney. Claudin-16 and claudin-19 expression is strongly reduced in kidneys of 2-month-old *KCTD1^{-/-}* and *Six2Cre⁺KCTD1^{fl/fl}* mice, whereas claudin-14 expression is increased. Expression of ATP1a1 or PTH1R is decreased in kidneys of 2-month-old *KCTD1^{-/-}* and *Six2Cre⁺KCTD1^{fl/fl}* mice but not at P3 before nephron maturation. Values normalized to their controls.
- (B) The expression of *CLCNKB* is increased in kidneys of 2-month-old *KCTD1^{-/-}* and *Six2Cre⁺KCTD1^{fl/fl}* mice. This is not observed before the manifestation of the distal nephron maturation defect (normal at P8). Values are normalized to their controls.
- (C) Total expression levels of claudin-16 and claudin-19 in kidneys of P3, P8, and 2-month-old *Six2Cre⁺KCTD1^{fl/fl}* mice and their littermate controls.
- (D) Semiquantitative RT-PCR analysis in kidneys of 2-month-old *KCTD1^{-/-}* and *Six2Cre⁺KCTD1^{fl/fl}* mice shows a significant decrease in *Slc34a1* and *Slc34a3* transcripts. Values normalized to their controls.
- (E) Semiquantitative RT-PCR analysis in kidneys of 2-month-old *KCTD1^{-/-}* and *Six2Cre⁺KCTD1^{fl/fl}* mice shows a significantly increased expression of the Ca^{2+} channels TRPV5 and TRPV6. *NCX1* and *calbindin-D_{28k}* expression is not reduced in kidneys lacking KCTD1. Values normalized to their controls.
- (F) Summary of expression changes of key regulators of urinary Ca^{2+} reabsorption shows similar results when comparing kidneys of 2-month-old *KCTD1^{-/-}* and *Six2Cre⁺KCTD1^{fl/fl}* mice.
- (G) Immunolabeling of kidneys from 6-month-old *Six2Cre⁺KCTD1^{fl/fl}* mice and their WT controls for active β -catenin, claudin-14, claudin-19, and TRPV5 shows localization of these proteins in dilated distal tubules of *Six2Cre⁺KCTD1^{fl/fl}* mice. DAPI stains nuclei blue. Scale bars, 20 μm
- Graphs represent data as means \pm SEM. Semiquantitative RT-PCRs performed in triplicate with $n > 6$ samples/group. p values are shown (two-tailed, unpaired t test).

that the reduction in expression of those claudins occurs only after the time when normal nephron terminal differentiation takes place (which is mainly in the first 2 weeks after birth): low-level expression of claudin-16 and -19, with no reduction compared with WT littermates, was detected at postnatal days 3 (P3) or 8 (P8) in kidneys of Six2Cre⁺KCTD1^{fl/fl} mice (during the early terminal differentiation phase), whereas 2-month-old Six2-Cre⁺KCTD1^{fl/fl} mice showed strongly decreased renal expression of claudin-16 and -19 (Figure 4C). These findings suggest that the diminished urinary Ca²⁺ and Mg²⁺ reabsorption in the TALs of mice lacking KCTD1 is a consequence of a progressive TAL defect.

The renal sodium phosphate co-transporters Npt2a (encoded by *Slc34a1*) and Npt2c (encoded by *Slc34a3*) in the apical brush border membrane of PTs are essential regulators of reabsorption of filtered phosphate (Blaine et al., 2015). PTH and FGF23 lead to an acute translocation of those phosphate co-transporters from the apical brush border membrane of PTs into the cytosol and thereby reduce reabsorption of filtered phosphate (Quarles, 2008). FGF23 reduces both the expression and the activity of those sodium phosphate co-transporters. Consistent with the increase in FGF23 in KCTD1^{-/-} and Six2Cre⁺KCTD1^{fl/fl} mice, expression of *Slc34a1* and *Slc34a3* was strongly reduced in the kidneys of these mice (Figure 4D).

Immunolabeling confirmed that dilated distal nephron tubules in adult Six2Cre⁺KCTD1^{fl/fl} mice showed strong staining for active β -catenin, particularly at the basal side of the epithelial cells, and for claudin-14 apically (consistent with its tight junction localization) (Figure 4G). Dilated TALs also showed immunolabeling for claudin-19 in these mice (Figure 4G).

Increased Expression of Ca²⁺ Transporters of DCT2s/CTs in KCTD1-Deficient Mice

Next, changes in expression of key genes involved in the regulation of transcellular Ca²⁺ transport in DCT2s were assessed to determine a possible contribution of DCT defects to the overall observed hypocalcemia in mice lacking KCTD1. The DCT2s reabsorb only a relatively small fraction of the filtered Ca²⁺ (~8%), whereas the TALs reabsorb ~25% of filtered Ca²⁺ (Blaine et al., 2015). Although urinary Ca²⁺ reabsorption occurs in TALs via a paracellular mechanism, DCT2s and CTs reabsorb urinary Ca²⁺ via a transcellular mechanism: apical Ca²⁺ transport in these nephron segments occurs via the TRPV5 Ca²⁺ channel (expressed in DCT2s and CTs), then Ca²⁺ associates with the Ca²⁺ binding protein calbindin-D_{28K}, which shuttles it to the basolateral surface, where it is extruded by the Ca²⁺ ATPase and the type 1 sodium calcium exchanger NCX1 (*Slc8a1*) (Subramanya and Ellison, 2014). TRPV5 activity has been suggested to be the rate-limiting step of reabsorption of filtered Ca²⁺ in DCT2s/CTs, whose expression is increased by PTH and FGF23 (Andrukhova et al., 2014; Cha et al., 2008; de Groot et al., 2009; van Abel et al., 2005).

Semiquantitative RT-PCR of whole kidneys shows that the Ca²⁺ transporters TRPV5 and TRPV6, which promote transcellular Ca²⁺ reabsorption mainly in the DCT2s/CTs, were significantly upregulated in the kidneys of KCTD1^{-/-} and Six2Cre⁺KCTD1^{fl/fl} mice, likely to counter the impaired urinary Ca²⁺ reabsorption in the TALs by increasing Ca²⁺ reabsorption in the DCT2s/CTs (Fig-

ure 4E). This increased TRPV5 expression may, to some extent, be due to the increase in PTH and FGF23 serum levels in these mice (Cha et al., 2008; de Groot et al., 2009). Moreover, calbindin-D_{28K} and NCX1 expression were not reduced in kidneys of KCTD1^{-/-} and Six2Cre⁺KCTD1^{fl/fl} mice (Figure 4E). Immunolabeling also confirmed increased TRPV5 in dilated tubules in kidneys of Six2Cre⁺KCTD1^{fl/fl} mice when compared with their WT littermates (Figure 4G). Thus, these findings suggest that urinary Ca²⁺ loss in those mice is explained mainly by impaired Ca²⁺ reabsorption in the TALs and not the DCT2s/CTs because key genes involved in Ca²⁺ transport in the DCT2s/CTs were either increased or unchanged, whereas key genes involved in Ca²⁺ transport in the TALs were strongly diminished (Figure 4F). Notably, the observation that both KCTD1^{-/-} and Six2-Cre⁺KCTD1^{fl/fl} mice showed similar relative expression changes for these regulators of Ca²⁺ reabsorption in the kidney demonstrates that these changes are a consequence of the lack of kidney-specific functions of KCTD1 and do not occur because of functions of KCTD1 in other organs (Figure 4F).

KCTD1 Mutants Develop Progressive Metabolic Bone Disease

Chronic secondary hyperparathyroidism can lead to high-turnover metabolic bone disease with the manifestation of osteitis fibrosa and decreased bone mineralization (Moor and Bonny, 2016). Because the sustained hypocalcemia in mice lacking KCTD1 led to chronic secondary hyperparathyroidism, it is likely that these mice would also develop progressive high-turnover metabolic bone disease. Indeed, histologic analyses of long bones (tibia and femur) revealed severe osteitis-fibrosa-like pathologies in aged KCTD1^{-/-} and Six2Cre⁺KCTD1^{fl/fl} mice but not in their control littermates (Figure 5A). Skeletal imaging by positron emission tomography-computed tomography (PET-CT) also showed delayed calvarial bone formation already in young KCTD1^{-/-} mice (Figure 5B). The high-turnover bone disease from chronic secondary hyperparathyroidism is characterized by increased activity of osteoclasts and osteoblasts and reduced bone mineralization (Moor and Bonny, 2016). Bone histomorphometric analysis of femurs of 6-week-old, male KCTD1^{-/-} mice that had increased PTH serum levels showed evidence for high-turnover bone disease already at that young age: those mice had increased osteoclast activity with higher eroded surface/bone surface, higher osteoclast surface/bone surface, higher osteoblast surface/bone surface, and higher osteoid/bone surface ratios (Figures 6A and 6B). Bone loss was observed as well with reduced bone volume/total volume ratio and reduced bone area (Figure 6B). These findings were also confirmed by micro-CT (μ CT) analyses and by von Kossa staining of tibias and femurs in these KCTD1^{-/-} mice, which showed reduced bone mineral density and bone loss with a significant reduction in trabecular and cortical bone (already seen at 6 weeks of age) (Figures 7A–7C). These bone findings are consistent with progressive metabolic bone disease from chronic secondary hyperparathyroidism.

DISCUSSION

It has been proposed that NCC is required for transcellular Mg²⁺ transport in DCT cells, in part by promoting Na⁺ influx into the

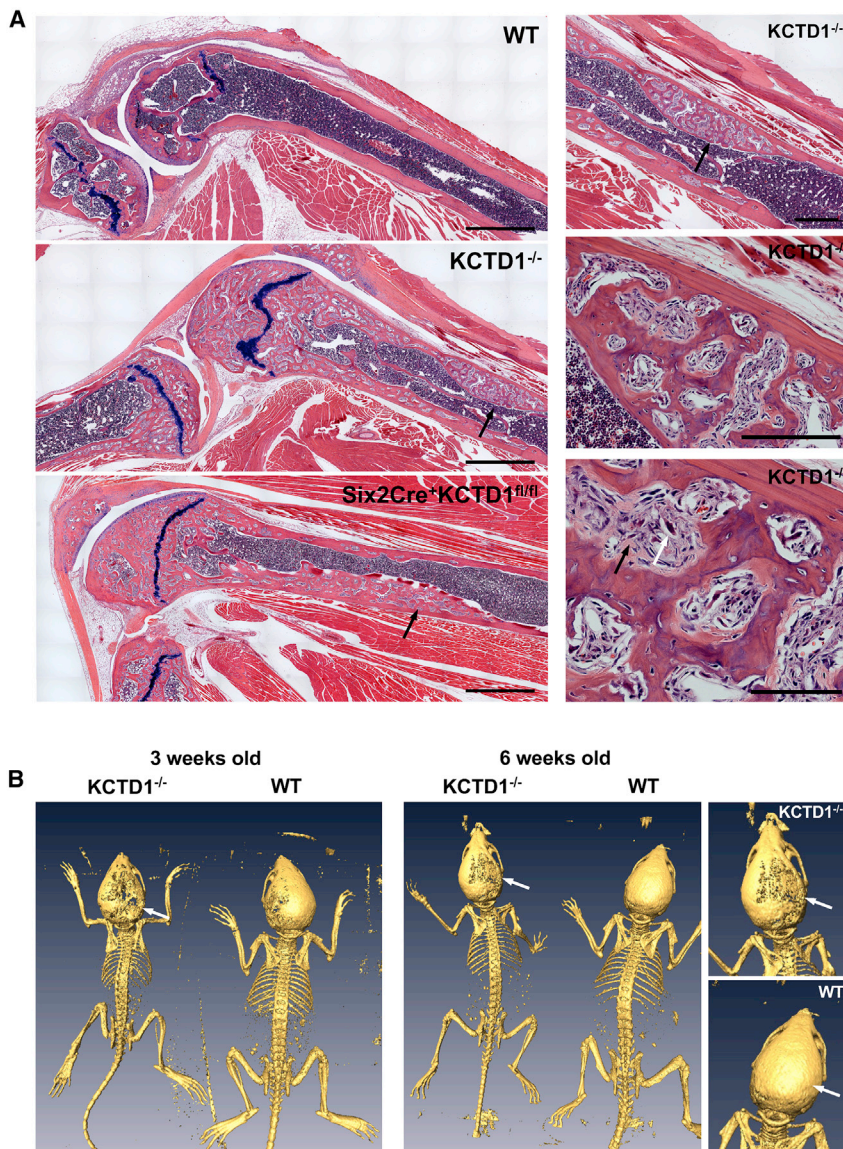


Figure 5. Severe Renal Osteodystrophy-like Bone Disease in Aged KCTD1^{-/-} and Six2-Cre⁺KCTD1^{fl/fl} Mice

(A) Left: knee joint with femur and tibia of a 12-month-old KCTD1^{-/-} mouse and its WT control is shown, as well as that of a 9-month-old Six2-Cre⁺KCTD1^{fl/fl} mouse. Both KCTD1^{-/-} and Six2-Cre⁺KCTD1^{fl/fl} mice show severely abnormal bone with increased fibrous tissue and osteoclasts (black arrows). Right: higher-magnification images of image from KCTD1^{-/-} mouse femur. Abnormal cortical bone with fibroblast-like cells (black arrow) and accumulation of osteoclasts (white arrow). H&E staining. Scale bars, left: 900 μ m; right: 500 μ m (top), 200 μ m (middle), 100 μ m (bottom).

(B) PET-CT imaging shows delayed calvarial ossification (arrows) when comparing 3- and 6-week-old male KCTD1^{-/-} mice with their littermate controls.

lead to an overall reduction of all DCT differentiation genes but particularly affects NCC. EGF deficiency did not lead to significant hypomagnesemia. Thus, EGF is not a rate-limiting magnesiotropic factor *in vivo*.

TALs reabsorb about 50%–60% of filtered Mg²⁺ and about 20% of filtered Ca²⁺ via the paracellular pathway (Mount, 2014). The importance of TALs for paracellular reabsorption of both urinary Mg²⁺ and Ca²⁺ is demonstrated by the observation of mutations in the tight junction genes for claudin-16 and claudin-19, which regulate paracellular transport of those cations in TALs in human disorders that manifest with hypomagnesemia and hypercalciuria (Konrad et al., 2006; Simon et al., 1999). As claudin-16 and claudin-19 are significantly downregulated in kidneys lacking KCTD1, it is likely that urinary Mg²⁺ wasting due to KCTD1 deficiency occurs as a consequence of both impaired trans-

cellular Mg²⁺ reabsorption in DCT1s and reduced paracellular Mg²⁺ uptake from urine in TALs. Collectively, these findings uncover a critical role for KCTD1 in DCT1s and TALs for overall Mg²⁺ homeostasis.

Moreover, these data demonstrate that KCTD1 is also required for the ability of TALs (and possibly to some extent DCT2s) to reabsorb filtered Ca²⁺ from urine. In addition to urinary Mg²⁺ wasting, KCTD1 deficiency also leads to urinary Ca²⁺ loss, resulting in hypocalcemia and consequently chronic secondary hyperparathyroidism with high-turnover metabolic bone disease already at an early age and that progresses to severe renal osteodystrophy-like pathologies in aged KCTD1 mutant mice. Kidneys lacking KCTD1 show diminished expression of TAL genes that regulate paracellular Ca²⁺ reabsorption, whereas genes that regulate transcellular Ca²⁺ reabsorption in DCT2s/CTs were increased (Figure 7D). This suggests that urinary Ca²⁺

cellular Mg²⁺ reabsorption in DCT1s and reduced paracellular Mg²⁺ uptake from urine in TALs. Collectively, these findings uncover a critical role for KCTD1 in DCT1s and TALs for overall Mg²⁺ homeostasis.

Moreover, these data demonstrate that KCTD1 is also required for the ability of TALs (and possibly to some extent DCT2s) to reabsorb filtered Ca²⁺ from urine. In addition to urinary Mg²⁺ wasting, KCTD1 deficiency also leads to urinary Ca²⁺ loss, resulting in hypocalcemia and consequently chronic secondary hyperparathyroidism with high-turnover metabolic bone disease already at an early age and that progresses to severe renal osteodystrophy-like pathologies in aged KCTD1 mutant mice. Kidneys lacking KCTD1 show diminished expression of TAL genes that regulate paracellular Ca²⁺ reabsorption, whereas genes that regulate transcellular Ca²⁺ reabsorption in DCT2s/CTs were increased (Figure 7D). This suggests that urinary Ca²⁺

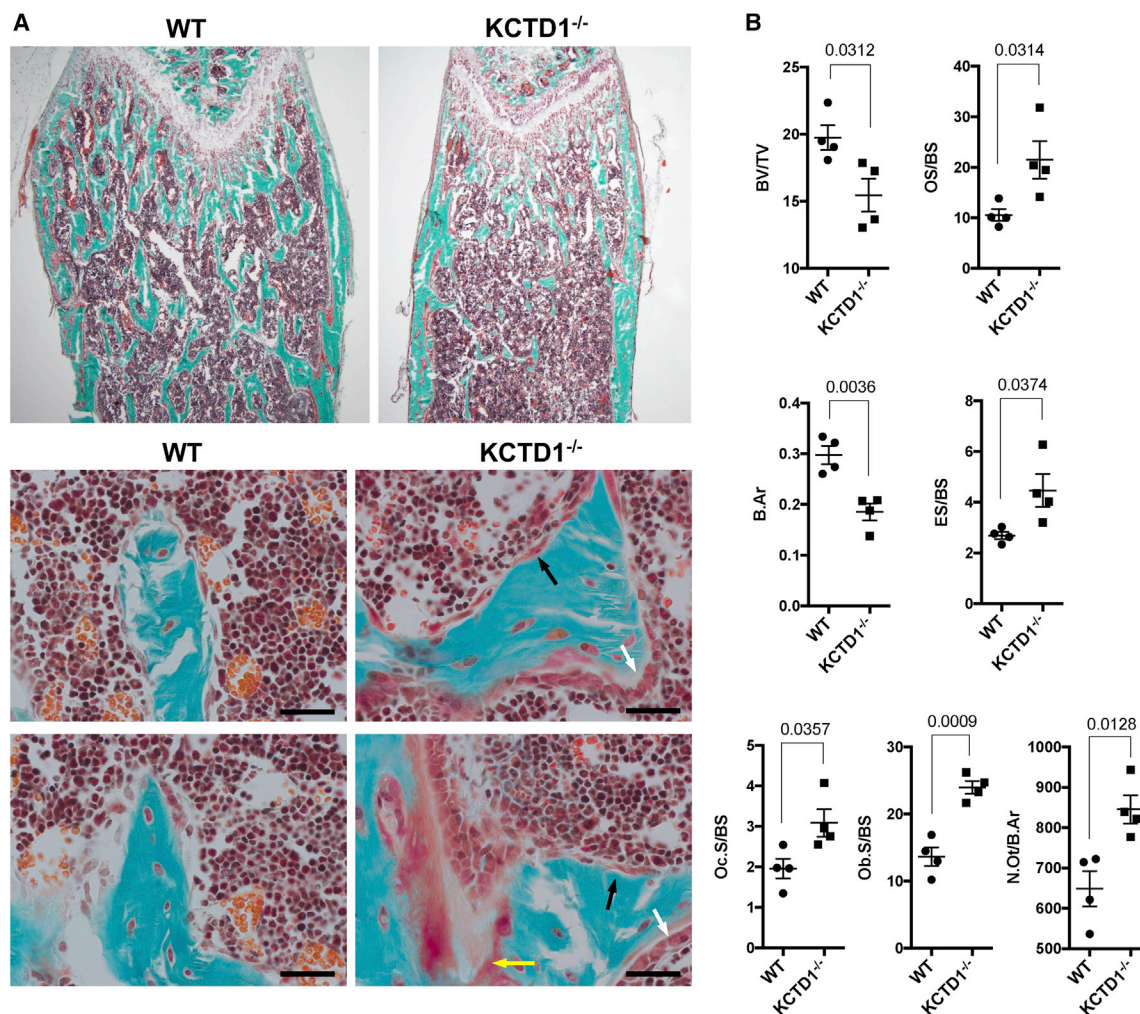


Figure 6. Bone Histomorphometric Analysis Shows High-turnover Metabolic Bone Disease Already in Young Mice Lacking KCTD1

(A) Goldner-trichrome-stained femur shows reduced bone in 6-week-old male KCTD1^{-/-} mice compared with WT control mice. An increase in osteoclasts (black arrows), osteoblasts (white arrows), and osteoid (yellow arrow) is observed in mice lacking KCTD1. Scale bars, 50 μ m.

(B) Bone histomorphometry findings in 6-week-old KCTD1^{-/-} and WT control mice. KCTD1^{-/-} mice show reduced bone (BV/TV and B.Ar), and increased osteoclasts (Oc.S/BS), osteoclast activity (ES/BS), osteoblasts (Ob.S/BS), and osteoid (OS/BS). BV/TV, bone volume/tissue volume; B.Ar, trabecular bone area; Oc.S, osteoclast surface/bone surface; Ob.S/BS, osteoblast surface/bone surface; ES/BS, eroded surface/bone surface; OS/BS, osteoid surface/bone surface. Graphs represent data as means \pm SEM. p values are shown (two-tailed, unpaired t test).

wasting and the associated abnormalities in calcium/phosphate metabolism are due to primarily insufficient paracellular Ca^{2+} transport in TALs. However, it is possible that transcellular Ca^{2+} uptake by DCT2 epithelial cells is also impaired in mice lacking KCTD1 and that the upregulation of TRPV5/TRPV6 is a compensatory mechanism without an actual functional increase of reabsorption of filtered Ca^{2+} in DCT2s. Nevertheless, it is more likely that the observed hypercalciuria is at least to a greater extent due to defects in TALs rather than DCT2s in mice lacking KCTD1 because the TALs contribute significantly more to reabsorption of filtered Ca^{2+} in the kidney, and the TAL transporters involved in this process were strongly diminished, whereas the DCT transporters involved in Ca^{2+} transport were increased.

The absence of urinary Ca^{2+} wasting in PvalbCre⁺KCTD1^{fl/fl} and Aqp2Cre⁺KCTD1^{fl/fl} mice shows that DCT1s and CTs/CDs

are not contributing to this phenotype of defective renal Ca^{2+} re-uptake; similarly, the lack of KCTD1 in PTGs or intestines had no effects on calcium/phosphate homeostasis. Six2Cre⁺KCTD1^{fl/fl} mice phenocopied KCTD1^{-/-} mice and showed very similar abnormalities in calcium/phosphate metabolism, demonstrating that these abnormalities are due to kidney-specific alterations and not due to potential roles of KCTD1 in other organs. In addition to the TALs, PTs are also a major site of Mg^{2+} and Ca^{2+} reabsorption. However, KCTD1 is not expressed in the PTs, which showed no morphological abnormalities in young adult KCTD1^{-/-} or Six2Cre⁺KCTD1^{fl/fl} mice that have already manifested urinary Mg^{2+} and Ca^{2+} loss. Nevertheless, the progressive impairment of overall renal function in kidneys lacking KCTD1 may contribute, to some extent, to the urinary Mg^{2+} and Ca^{2+} loss as well.

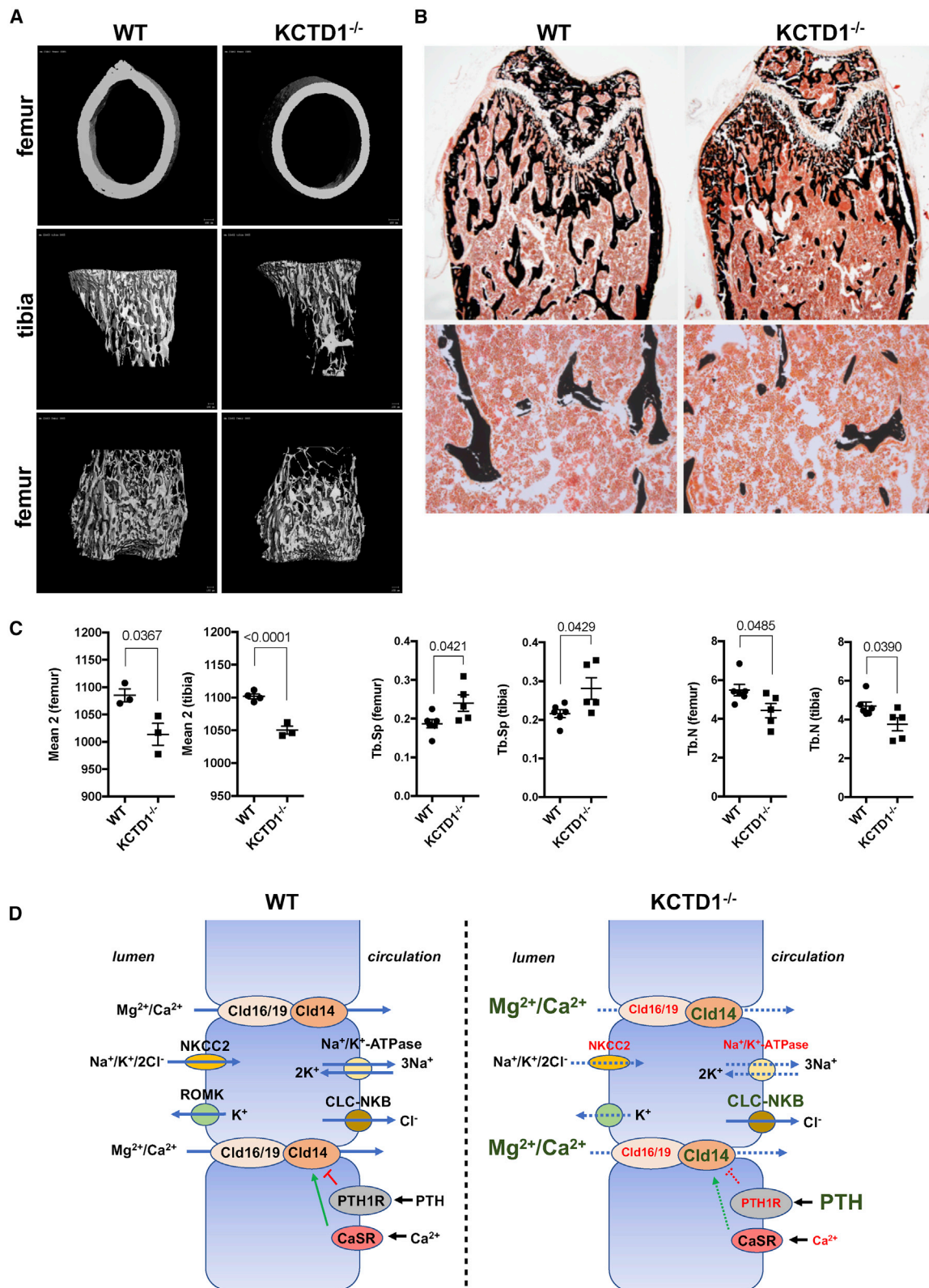


Figure 7. Reduced Bone Volume and Bone Mineral Density due to KCTD1 Deficiency

(A) Reduced mineralized bone is observed by μ CT imaging of the long bones in 6-week-old, male KCTD1^{-/-} mice compared with control littermate mice.

(B) Von Kossa-stained femurs from the mice analyzed by μ CT show diminished bone in KCTD1^{-/-} mice.

(legend continued on next page)

Paracellular Ca^{2+} and Mg^{2+} reabsorption from the TAL lumen into the circulation requires a lumen-positive transepithelial electrical gradient that is generated by a NKCC2-mediated influx of $\text{Na}^+/\text{K}^+/\text{Cl}^-$ ions into TAL epithelial cells and the concomitant efflux of K^+ ions back into the tubular lumen through the inward-rectifier K^+ -channel ROMK (KCNJ1) (Moor and Bonny, 2016). Although NKCC2 and ROMK are localized at the apical site of the TAL epithelial cells, the Na^+/K^+ -ATPase and the chloride channel CLC-NKB are located at the basolateral site and are required for Na^+ and Cl^- transport, respectively, into the circulation (in addition a K^+ channel and a K^+/Cl^- cotransporter are present). The overall net effect of these transporters is that a lumen-positive electrical gradient drives paracellular Ca^{2+} and Mg^{2+} transport from the tubular lumen of the TAL into the circulation (Mount, 2014). The critical roles of NKCC2 and ROMK for paracellular Ca^{2+} reabsorption in the TALs are well established because mutations in their genes in Bartter syndrome lead to hypercalciuria, hyperparathyroidism, and osteopenia (and a subset of patients also develop hypomagnesemia) (Simon et al., 1996a, 1996b), and mice with NKCC2 mutations develop hypercalciuria and osteopenia as well (Kemter et al., 2010). TAL defects as a consequence of the lack of KCTD1 were associated with diminished expression of NKCC2 and ATP1A1 in kidneys of both $\text{KCTD1}^{-/-}$ and $\text{Six2Cre}^+\text{KCTD1}^{\text{fl/fl}}$ mice. These changes would be expected to reduce the transepithelial electrical gradient that is required for paracellular Mg^{2+} and Ca^{2+} transport in the TAL, explaining, at least in part, the urinary Mg^{2+} and Ca^{2+} loss in mice lacking KCTD1, which leads to secondary hyperparathyroidism and metabolic bone disease, resembling findings in patients with Bartter syndrome (Figure 7D).

Paracellular Ca^{2+} and Mg^{2+} transport in TALs is also regulated by specific claudins (Moor and Bonny, 2016). Claudin-16 and claudin-19 are hemichannels that form a paracellular pore in TALs through which Mg^{2+} and Ca^{2+} transport occurs. Patients with mutations in these genes develop hypomagnesemia and hypercalciuria (Konrad et al., 2006; Simon et al., 1999). Mice lacking claudin-16 manifested urinary Ca^{2+} and Mg^{2+} wasting and compensatory increased expression of TRPV5 and TRPV6, which can form heteromultimers and serve as apical channels for transcellular Ca^{2+} transport into the epithelial cells of DCT2s/CTs (Hou et al., 2007; Will et al., 2010).

The tight junction protein claudin-14 interacts with claudin-16 and interferes with paracellular Ca^{2+} and Mg^{2+} reabsorption in the TALs (claudins 14, 16, and 19 are highly expressed in TALs [Park et al., 2018; Ransick et al., 2019]), whereas loss of claudin-14 results in increased Ca^{2+} and Mg^{2+} reabsorption, which leads to hypermagnesemia and hypocalciuria (Gong et al., 2012). Ca^{2+} reabsorption in TALs is stimulated by PTH/PTH1R signaling through a mechanism that suppresses claudin-14 expression and induces its cytosolic translocation from the tight junction (Sato et al., 2017). Consistent with those findings, uri-

nary Ca^{2+} wasting in $\text{KCTD1}^{-/-}$ and $\text{Six2Cre}^+\text{KCTD1}^{\text{fl/fl}}$ mice was associated with decreased renal expression of PTH1R and claudins-16 and -19 and increased expression of claudin-14. Moreover, a compensatory increase in expression of TRPV5 and TRPV6 was observed in kidneys of these mice. PTH and FGF23 both increase expression of TRPV5 in DCT2s/CTs (Andrukhova et al., 2014; de Groot et al., 2009; van Abel et al., 2005), explaining the compensatory increase in its expression observed in mice lacking KCTD1, which have increased PTH and FGF23. Collectively, these findings provide evidence that a defect primarily in paracellular Ca^{2+} reabsorption in the TALs contributes to the urinary Ca^{2+} loss in $\text{KCTD1}^{-/-}$ and $\text{Six2Cre}^+\text{KCTD1}^{\text{fl/fl}}$ mice.

Notably, PTH1R is expressed in podocytes, PTs, TALs, DCTs, and CTs, and overall renal expression of PTH1R was reduced in 2-month-old $\text{KCTD1}^{-/-}$ and $\text{Six2Cre}^+\text{KCTD1}^{\text{fl/fl}}$ mice (Ransick et al., 2019). The absence of KCTD1 in podocytes and PTs and their normal morphology in young KCTD1 mutants suggests that PTH1R function in PTs may be normal and properly regulates the activity of the renal sodium phosphate co-transporters Npt2a and Npt2c (explaining their downregulation with increased PTH levels in these mice). Alternatively, even if PTH1R activity in PTs would be reduced, the increase in FGF23 in $\text{KCTD1}^{-/-}$ and $\text{Six2Cre}^+\text{KCTD1}^{\text{fl/fl}}$ mice would explain the decreased expression of these sodium phosphate co-transporters in PTs as well. Similarly, should PTH1R expression also be reduced in DCT2s, the increase in TRPV5/TRPV6 expression could be explained by increased FGF23. Thus, the observation of reduced expression of Npt2a and Npt2c genes in the PTs and increased TRPV5/TRPV6 in DCT2s and increased claudin-14 in TALs would be explained by increased serum FGF23 and PTH levels even if PTH1R would not only be diminished in TALs.

In CKD, phosphate excretion and phosphate serum levels are initially maintained within a normal range through a decrease in reabsorption of phosphate in PTs, which is mediated by the inhibitory effects of PTH and FGF23 on Npt2a and Npt2c. Similarly, the increase in PTH and FGF23 in both $\text{KCTD1}^{-/-}$ and $\text{Six2Cre}^+\text{KCTD1}^{\text{fl/fl}}$ mice was associated with decreased expression of these sodium phosphate co-transporters. However, with deterioration of kidney function in patients with more advanced CKD, this compensatory mechanism is not sufficient, and hyperphosphatemia develops. In particular, serum levels of the main phosphaturic hormone FGF23 are already increased early in the disease course of CKD and precede a detectable increase in serum phosphate levels. This observation seen in CKD patients was also observed in $\text{KCTD1}^{-/-}$ mice: young KCTD1 -deficient mice showed a strong increase in FGF23 when serum phosphate levels were still normal, but aged $\text{KCTD1}^{-/-}$ mice with more severe renal abnormalities had highly increased serum phosphate levels. Similarly, metabolic bone disease can develop at early stages of CKD and progress with further deterioration of

(C) Reduced bone density (mean 2) and trabecular bone (Tb.N) with increased trabecular spaces (Tb.Sp) observed by μCT imaging of long bones in 6-week-old, male $\text{KCTD1}^{-/-}$ mice compared with control littermates.

(D) Proposed pathomechanisms through which KCTD1 deficiency impairs paracellular urinary Mg^{2+} and Ca^{2+} reabsorption in TALs and thereby leads to secondary hyperparathyroidism and metabolic bone disease. Genes with reduced expression are indicated in a smaller red font; genes with increased expression are in an enlarged green font.

Graphs represent data as means \pm SEM. p values are shown (two-tailed, unpaired t test).

kidney function. Mice lacking KCTD1 also developed bone loss and reduced bone mineralization already at an early age. Secondary hyperparathyroidism is also a relatively early consequence of kidney impairment in CKD and increased PTH concentrations can be observed when serum levels of calcium or phosphate are still within the normal range. Similarly, KCTD1^{-/-} mice had increased PTH serum levels already at a young age. The high PTH levels in KCTD1 mutants are likely due to a combination of phosphate retention as a consequence of progressive renal insufficiency and hypocalcemia because of impaired urinary Ca²⁺ reabsorption.

Bone pathologies in KCTD1 mutants show high-turnover metabolic bone disease with features of osteitis fibrosa cystica or mixed uremic osteodystrophy, such as the loss of bone volume and reduced bone mineralization. Osteitis fibrosa cystica shows an increase in the number and activity of osteoblasts and osteoclasts and an increase in osteoid. Lack of KCTD1 resulted in increased osteoid, osteoclasts, and osteoblasts and in reduced bone mineralization. Thus, the lack of KCTD1 causes secondary hyperparathyroidism, which results in high-turnover bone disease with the typical features of metabolic bone disease seen in CKD. Overall, the temporal changes in calcium/phosphate and bone metabolism observed in mice lacking KCTD1 show many similarities to clinical observations in CKD. Notably, the metabolic bone disease in KCTD1^{-/-} and Six2Cre⁺KCTD1^{fl/fl} mice occurs not only in the setting of chronic hyperparathyroidism but also in the setting of progressive renal insufficiency with marked morphological renal abnormalities and a salt-losing tubulopathy. Thus, it is likely that the observed bone abnormalities in KCTD1 mutants are a consequence of the combination of those renal abnormalities and are not explained exclusively by hypocalcemia. In summary, these findings identify KCTD1 as a critical regulator of TAL/DCT function and as being essential for the ability of the kidney to reabsorb filtered Mg²⁺ and Ca²⁺ and control overall magnesium and calcium/phosphate metabolism.

STAR★METHODS

Detailed methods are provided in the online version of this paper and include the following:

- KEY RESOURCES TABLE
- RESOURCE AVAILABILITY
 - Lead Contact
 - Materials Availability
 - Data and Code Availability
- EXPERIMENTAL MODEL AND SUBJECT DETAILS
- METHOD DETAILS
 - Western blotting
 - Immunolabeling of kidney sections and morphological kidney analyses
 - Semiquantitative RT-PCR
 - ELISAs, serum and urine chemistries
 - Bone analyses
- QUANTIFICATION AND STATISTICAL ANALYSIS
 - RNA-seq data analysis
 - Statistics

SUPPLEMENTAL INFORMATION

Supplemental Information can be found online at <https://doi.org/10.1016/j.celrep.2020.108616>.

ACKNOWLEDGMENTS

The author would like to thank Karin Strittmatter and Janaina Da Silva Martins for technical assistance and Michael Mannstadt for critical reading of this manuscript. Services of the Harvard School of Dental Medicine Micro CT Core Facility and of the NIH-sponsored Center for Skeletal Research Core (NIH P30 AR066261) at Massachusetts General Hospital are acknowledged. This study was supported by institutional funds and by funding from the NIH (R01DK118134, R01DK121178, and R21AG063377) to A.G.M.

AUTHOR CONTRIBUTIONS

A.G.M. conceived and executed the project and wrote the manuscript.

DECLARATION OF INTERESTS

The author declares no competing interests.

Received: June 18, 2020

Revised: October 31, 2020

Accepted: December 17, 2020

Published: January 12, 2021

REFERENCES

- Andrukhoa, O., Smorodchenko, A., Egerbacher, M., Streicher, C., Zeitz, U., Goetz, R., Shalhoub, V., Mohammadi, M., Pohl, E.E., Lanske, B., and Erben, R.G. (2014). FGF23 promotes renal calcium reabsorption through the TRPV5 channel. *EMBO J.* 33, 229–246.
- Belge, H., Gailly, P., Schwaller, B., Loffing, J., Debaix, H., Riveira-Munoz, E., Beauwens, R., Devogelaer, J.P., Hoenderop, J.G., Bindels, R.J., and Devuyt, O. (2007). Renal expression of parvalbumin is critical for NaCl handling and response to diuretics. *Proc. Natl. Acad. Sci. USA* 104, 14849–14854.
- Blaine, J., Chonchol, M., and Levi, M. (2015). Renal control of calcium, phosphate, and magnesium homeostasis. *Clin. J. Am. Soc. Nephrol.* 10, 1257–1272.
- Cha, S.K., Wu, T., and Huang, C.L. (2008). Protein kinase C inhibits caveolae-mediated endocytosis of TRPV5. *Am. J. Physiol. Renal Physiol.* 294, F1212–F1221.
- de Groot, T., Lee, K., Langeslag, M., Xi, Q., Jalink, K., Bindels, R.J., and Hoenderop, J.G. (2009). Parathyroid hormone activates TRPV5 via PKA-dependent phosphorylation. *J. Am. Soc. Nephrol.* 20, 1693–1704.
- Dempster, D.W., Compston, J.E., Drezner, M.K., Glorieux, F.H., Kanis, J.A., Malluche, H., Meunier, P.J., Ott, S.M., Recker, R.R., and Parfitt, A.M. (2013). Standardized nomenclature, symbols, and units for bone histomorphometry: a 2012 update of the report of the ASBMR Histomorphometry Nomenclature Committee. *J. Bone Miner. Res.* 28, 2–17.
- Ding, X.F., Luo, C., Ren, K.Q., Zhang, J., Zhou, J.L., Hu, X., Liu, R.S., Wang, Y., Gao, X., and Zhang, J. (2008). Characterization and expression of a human KCTD1 gene containing the BTB domain, which mediates transcriptional repression and homomeric interactions. *DNA Cell Biol.* 27, 257–265.
- Ding, X., Luo, C., Zhou, J., Zhong, Y., Hu, X., Zhou, F., Ren, K., Gan, L., He, A., Zhu, J., et al. (2009). The interaction of KCTD1 with transcription factor AP-2alpha inhibits its transactivation. *J. Cell. Biochem.* 106, 285–295.
- Gong, Y., Renigunta, V., Himmerkus, N., Zhang, J., Renigunta, A., Bleich, M., and Hou, J. (2012). Claudin-14 regulates renal Ca⁺⁺ transport in response to CaSR signalling via a novel microRNA pathway. *EMBO J.* 31, 1999–2012.
- Grimm, P.R., Coleman, R., Delpire, E., and Welling, P.A. (2017). Constitutively Active SPAK Causes Hyperkalemia by Activating NCC and Remodeling Distal Tubules. *J. Am. Soc. Nephrol.* 28, 2597–2606.

- Groenestege, W.M., Thébaud, S., van der Wijst, J., van den Berg, D., Janssen, R., Tejpar, S., van den Heuvel, L.P., van Cutsem, E., Hoenderop, J.G., Knoers, N.V., and Bindels, R.J. (2007). Impaired basolateral sorting of pro-EGF causes isolated recessive renal hypomagnesemia. *J. Clin. Invest.* **117**, 2260–2267.
- Hayashi, S., and McMahon, A.P. (2002). Efficient recombination in diverse tissues by a tamoxifen-inducible form of Cre: a tool for temporally regulated gene activation/inactivation in the mouse. *Dev. Biol.* **244**, 305–318.
- Hou, J., Shan, Q., Wang, T., Gomes, A.S., Yan, Q., Paul, D.L., Bleich, M., and Goodenough, D.A. (2007). Transgenic RNAi depletion of claudin-16 and the renal handling of magnesium. *J. Biol. Chem.* **282**, 17114–17122.
- Kemter, E., Rathkolb, B., Bankir, L., Schrewe, A., Hans, W., Landbrecht, C., Klaffen, M., Ivandic, B., Fuchs, H., Gailus-Durner, V., et al. (2010). Mutation of the Na(+)-K(+)-2Cl(-) cotransporter NKCC2 in mice is associated with severe polyuria and a urea-selective concentrating defect without hyperreninemia. *Am. J. Physiol. Renal Physiol.* **298**, F1405–F1415.
- Kobayashi, A., Valerius, M.T., Mugford, J.W., Carroll, T.J., Self, M., Oliver, G., and McMahon, A.P. (2008). Six2 defines and regulates a multipotent self-renewing nephron progenitor population throughout mammalian kidney development. *Cell Stem Cell* **3**, 169–181.
- Konrad, M., Schaller, A., Seelow, D., Pandey, A.V., Waldegger, S., Lesslauer, A., Vitzthum, H., Suzuki, Y., Luk, J.M., Becker, C., et al. (2006). Mutations in the tight-junction gene claudin 19 (CLDN19) are associated with renal magnesium wasting, renal failure, and severe ocular involvement. *Am. J. Hum. Genet.* **79**, 949–957.
- Li, X., Chen, C., Wang, F., Huang, W., Liang, Z., Xiao, Y., Wei, K., Wan, Z., Hu, X., Xiang, S., et al. (2014). KCTD1 suppresses canonical Wnt signaling pathway by enhancing β -catenin degradation. *PLoS ONE* **9**, e94343.
- Libutti, S.K., Crabtree, J.S., Lorang, D., Burns, A.L., Mazzanti, C., Hewitt, S.M., O'Connor, S., Ward, J.M., Emmert-Buck, M.R., Remaley, A., et al. (2003). Parathyroid gland-specific deletion of the mouse *Men1* gene results in parathyroid neoplasia and hypercalcemic hyperparathyroidism. *Cancer Res.* **63**, 8022–8028.
- Lindström, N.O., De Sena Brandine, G., Tran, T., Ransick, A., Suh, G., Guo, J., Kim, A.D., Parvez, R.K., Ruffins, S.W., Rutledge, E.A., et al. (2018). Progressive Recruitment of Mesenchymal Progenitors Reveals a Time-Dependent Process of Cell Fate Acquisition in Mouse and Human Nephrogenesis. *Dev. Cell* **45**, 651–660.e4.
- Loffing, J., Loffing-Cueni, D., Valderrabano, V., Kläusli, L., Hebert, S.C., Rossier, B.C., Hoenderop, J.G., Bindels, R.J., and Kaissling, B. (2001). Distribution of transcellular calcium and sodium transport pathways along mouse distal nephron. *Am. J. Physiol. Renal Physiol.* **281**, F1021–F1027.
- Luetke, N.C., Qiu, T.H., Fenton, S.E., Troyer, K.L., Riedel, R.F., Chang, A., and Lee, D.C. (1999). Targeted inactivation of the EGF and amphiregulin genes reveals distinct roles for EGF receptor ligands in mouse mammary gland development. *Development* **126**, 2739–2750.
- Mameros, A.G. (2020). AP-2 β /KCTD1 control distal nephron differentiation and protect against renal fibrosis. *Dev. Cell* **54**, 348–366.e5.
- Mameros, A.G., Beck, A.E., Turner, E.H., McMillin, M.J., Edwards, M.J., Field, M., de Macena Sobreira, N.L., Perez, A.B., Fortes, J.A., Lampe, A.K., et al.; University of Washington Center for Mendelian Genomics (2013). Mutations in KCTD1 cause scalp-ear-nipple syndrome. *Am. J. Hum. Genet.* **92**, 621–626.
- Martin, K.J., and González, E.A. (2007). Metabolic bone disease in chronic kidney disease. *J. Am. Soc. Nephrol.* **18**, 875–885.
- Moor, M.B., and Bonny, O. (2016). Ways of calcium reabsorption in the kidney. *Am. J. Physiol. Renal Physiol.* **310**, F1337–F1350.
- Mount, D.B. (2014). Thick ascending limb of the loop of Henle. *Clin. J. Am. Soc. Nephrol.* **9**, 1974–1986.
- Park, J., Shrestha, R., Qiu, C., Kondo, A., Huang, S., Werth, M., Li, M., Barasch, J., and Suszták, K. (2018). Single-cell transcriptomics of the mouse kidney reveals potential cellular targets of kidney disease. *Science* **360**, 758–763.
- Quarles, L.D. (2008). Endocrine functions of bone in mineral metabolism regulation. *J. Clin. Invest.* **118**, 3820–3828.
- Ransick, A., Lindström, N.O., Liu, J., Zhu, Q., Guo, J.J., Alvarado, G.F., Kim, A.D., Black, H.G., Kim, J., and McMahon, A.P. (2019). Single-cell profiling reveals sex, lineage, and regional diversity in the mouse kidney. *Dev. Cell* **51**, 399–413.e7.
- Sato, T., Courbebaisse, M., Ide, N., Fan, Y., Hanai, J.I., Kaludjerovic, J., Den-smore, M.J., Yuan, Q., Toka, H.R., Pollak, M.R., et al. (2017). Parathyroid hormone controls paracellular Ca²⁺ transport in the thick ascending limb by regulating the tight-junction protein Claudin14. *Proc. Natl. Acad. Sci. USA* **114**, E3344–E3353.
- Schlingmann, K.P., Weber, S., Peters, M., Niemann Nejsum, L., Vitzthum, H., Klingel, K., Kratz, M., Haddad, E., Ristoff, E., Dinour, D., et al. (2002). Hypomagnesemia with secondary hypocalcemia is caused by mutations in TRPM6, a new member of the TRPM gene family. *Nat. Genet.* **31**, 166–170.
- Schultheis, P.J., Lorenz, J.N., Meneton, P., Nieman, M.L., Riddle, T.M., Flagella, M., Duffy, J.J., Doetschman, T., Miller, M.L., and Shull, G.E. (1998). Phenotype resembling Gitelman's syndrome in mice lacking the apical Na+Cl- cotransporter of the distal convoluted tubule. *J. Biol. Chem.* **273**, 29150–29155.
- Simon, D.B., Karet, F.E., Hamdan, J.M., DiPietro, A., Sanjad, S.A., and Lifton, R.P. (1996a). Bartter's syndrome, hypokalaemic alkalosis with hypercalciuria, is caused by mutations in the Na-K-2Cl cotransporter NKCC2. *Nat. Genet.* **13**, 183–188.
- Simon, D.B., Karet, F.E., Rodriguez-Soriano, J., Hamdan, J.H., DiPietro, A., Trachtman, H., Sanjad, S.A., and Lifton, R.P. (1996b). Genetic heterogeneity of Bartter's syndrome revealed by mutations in the K+ channel, ROMK. *Nat. Genet.* **14**, 152–156.
- Simon, D.B., Nelson-Williams, C., Bia, M.J., Ellison, D., Karet, F.E., Molina, A.M., Vaara, I., Iwata, F., Cushner, H.M., Koolen, M., et al. (1996c). Gitelman's variant of Bartter's syndrome, inherited hypokalaemic alkalosis, is caused by mutations in the thiazide-sensitive Na-Cl cotransporter. *Nat. Genet.* **12**, 24–30.
- Simon, D.B., Lu, Y., Choate, K.A., Velazquez, H., Al-Sabban, E., Praga, M., Casari, G., Bettinelli, A., Colussi, G., Rodriguez-Soriano, J., et al. (1999). Paracellin-1, a renal tight junction protein required for paracellular Mg²⁺ resorption. *Science* **285**, 103–106.
- Subramanya, A.R., and Ellison, D.H. (2014). Distal convoluted tubule. *Clin. J. Am. Soc. Nephrol.* **9**, 2147–2163.
- van Abel, M., Hoenderop, J.G., van der Kemp, A.W., Friedlaender, M.M., van Leeuwen, J.P., and Bindels, R.J. (2005). Coordinated control of renal Ca(2+) transport proteins by parathyroid hormone. *Kidney Int.* **68**, 1708–1721.
- Van Otterloo, E., Li, H., Jones, K.L., and Williams, T. (2018). AP-2 α and AP-2 β cooperatively orchestrate homeobox gene expression during branchial arch patterning. *Development* **145**, dev157438.
- Voets, T., Nilius, B., Hoefs, S., van der Kemp, A.W., Droogmans, G., Bindels, R.J., and Hoenderop, J.G. (2004). TRPM6 forms the Mg²⁺ influx channel involved in intestinal and renal Mg²⁺ absorption. *J. Biol. Chem.* **279**, 19–25.
- Walder, R.Y., Landau, D., Meyer, P., Shalev, H., Tsoia, M., Borochoowitz, Z., Boettger, M.B., Beck, G.E., Englehardt, R.K., Carmi, R., and Sheffield, V.C. (2002). Mutation of TRPM6 causes familial hypomagnesemia with secondary hypocalcemia. *Nat. Genet.* **31**, 171–174.
- Will, C., Breiderhoff, T., Thumfart, J., Stuiver, M., Kopplin, K., Sommer, K., Günzel, D., Querfeld, U., Meij, I.C., Shan, Q., et al. (2010). Targeted deletion of murine *Cldn16* identifies extra- and intrarenal compensatory mechanisms of Ca²⁺ and Mg²⁺ wasting. *Am. J. Physiol. Renal Physiol.* **298**, F1152–F1161.
- Xi, Q., Hoenderop, J.G., and Bindels, R.J. (2009). Regulation of magnesium reabsorption in DCT. *Pflügers Arch.* **458**, 89–98.

STAR★METHODS

KEY RESOURCES TABLE

REAGENT or RESOURCE	SOURCE	IDENTIFIER
Antibodies		
rabbit anti- β -galactosidase	Thermo Fisher Scientific	Cat# A-11132, RRID:AB_221539
rabbit anti-TRPM6	Thermo Fisher Scientific	Cat# PA5-77326, RRID:AB_2736741
rabbit anti-TRPV5	MyBiosource	Cat# MBS9125453
rabbit anti-Cldn14	MyBiosource	Cat# MBS1494658
rabbit anti-Cldn19	BiCell Scientific	Cat# 00219
chicken anti- β -galactosidase	Abcam	Cat# ab9361, RRID:AB_307210
goat anti-Aqp2	Santa Cruz Biotechnology	Cat# sc-9882, RRID:AB_2289903
rabbit anti-NCC	Millipore	Cat# AB3553, RRID:AB_571116
goat anti-THP	Santa Cruz Biotechnology	Cat# sc-19554, RRID:AB_793728
rabbit anti-GFP	Thermo Fisher Scientific	Cat# A-11122, RRID:AB_221569
rabbit anti-NKCC2	Cell Signaling Technologies	Cat# 38436, RRID:AB_2799134
rabbit anti-parvalbumin	Abcam	Cat# ab11427, RRID:AB_298032
goat anti-EGF	R&D Systems	Cat# AF2028, RRID:AB_355111
rabbit anti- β -actin antibody	Cell Signaling Technology	Cat# 4970, RRID:AB_2223172
rabbit anti-active β -catenin (non-phospho Ser33/37/Thr41)	Cell Signaling Technology	Cat# 8814S, RRID:AB_11127203
Chemicals, Peptides, and Recombinant Proteins		
tamoxifen	Sigma Aldrich	T5648
Critical Commercial Assays		
mouse 1,25 (OH) ₂ vitamin D ₃ EIA kit	ImmunoDiagnosticSystems PLC, Tyne and Wear, UK	Cat# AC-62F1
mouse FGF23 Immutopics ELISA Kit	Quidel, San Diego, USA	Cat# 60-6300
mouse PTH (PTH 1-84) ELISA kit	Quidel, San Diego, USA	Cat# 60-2305
Deposited Data		
RNA-seq data	Marneros, 2020	GEO: GSE126326
RNA-seq data	Marneros, 2020	GEO: GSE130864
Experimental Models: Organisms/Strains		
KCTD1 ^{-/-} mice and KCTD1 ^{fl/fl} mice	Marneros, 2020	N/A
Six2Cre ⁺ mice	Kobayashi et al., 2008	JAX:009606
PvalbCre ⁺ mice	Grimm et al., 2017	JAX:017320
Aqp2Cre ⁺ mice	Jackson Labs	JAX:006881
VilCre ⁺ mice	Jackson Labs	JAX:004586
PTHCre ⁺ mice	Libutti et al., 2003	JAX:005989
B6.Cg-Gt(ROSA)26Sor ^{tm3(CAG-EYFP)Hze/J} (Ai3)	Jackson Labs	JAX:007903
CAGGCreERT2 ⁺ mice	Hayashi and McMahon, 2002	JAX:004453
EGF ^{-/-} mice	Luetteke et al., 1999	N/A
TFAP2B ^{fl/fl} mice	Van Otterloo et al., 2018	N/A
Oligonucleotides		
semiquantitative RT-PCR primers	Life Technologies	See Table S1
Other		
rhodamine-conjugated peanut agglutinin	Vector Laboratories	Cat# RL-1072, RRID:AB_2336642
metabolic cages	Techniplast	3600M021
phalloidin conjugated with Alexa647	Thermo Fisher Scientific	Cat# A22287, RRID:AB_2620155

RESOURCE AVAILABILITY

Lead Contact

Further information and requests for resources and reagents should be directed to and will be fulfilled by the Lead Contact, Alexander G. Marneros (amarneros@mgh.harvard.edu).

Materials Availability

Mouse lines generated in this study are available upon request.

Data and Code Availability

RNA-seq data has been deposited to the GEO database: GSE126326 and GSE130864.

EXPERIMENTAL MODEL AND SUBJECT DETAILS

KCTD1-reporter mice, KCTD1^{-/-} mice, as well as mice with floxed KCTD1 alleles were generated as previously reported (Marneros, 2020). KCTD1^{fl/fl} mice were crossed with several Cre lines: Six2Cre⁺ mice (Kobayashi et al., 2008), PvalbCre⁺ mice (IMSR Cat# JAX:008069, RRID:IMSR_JAX:008069) (Grimm et al., 2017), Aqp2Cre⁺ mice [IMSR Cat# JAX:006881, RRID:IMSR_JAX:006881; using only female Aqp2Cre⁺ mice for matings], VilCre⁺ mice (IMSR Cat# JAX:004586, RRID:IMSR_JAX:004586), and PTH-Cre⁺ mice (Libutti et al., 2003) (IMSR Cat# JAX:005989, RRID:IMSR_JAX:005989) in order to obtain mice that are homozygous for the KCTD1^{fl/fl} allele and heterozygous for the corresponding Cre to establish cell type-specific conditional KCTD1 KO mice. Cre activity and specificity were confirmed by crossing these strains with an EYFP-reporter strain (B6.Cg-Gt(ROSA)26Sor^{tm3(CAG-EYFP)Hze}/J (Ai3) reporter mice; IMSR Cat# JAX:007903, RRID:IMSR_JAX:007903). Induced inactivation of KCTD1 in the adult (at 6-weeks of age) was achieved in β -actinCreERT2⁺KCTD1^{fl/fl} mice (generated by crossing CAGGCreERT2⁺ mice [IMSR Cat# JAX:004682, RRID:IMSR_JAX:004682] (Hayashi and McMahon, 2002) with KCTD1^{fl/fl} mice) with injection of tamoxifen (TAM) (6mg/40 gm BW daily for 5 consecutive days IP), a tamoxifen administration regimen that has been shown to efficiently and uniformly activate Cre recombinase in the kidney (Hayashi and McMahon, 2002). Efficient Cre-mediated removal of exon 3 of KCTD1 with this treatment regimen was confirmed by semiquantitative RT-PCR (one primer within exon 3) (Marneros, 2020). TFAP2B^{fl/fl} mice were kindly provided by Dr. Trevor Williams. The generation of these mice has previously been described: Cre-mediated recombination results in removal of exon 6 that is critical for DNA binding, resulting in TFAP2B without transcription factor activity (Van Otterloo et al., 2018). These mice were crossed with PvalbCre⁺ mice or β -actinCreERT2⁺KCTD1^{fl/fl} mice. The generation of EGF^{-/-} mice has previously been described (Luetke et al., 1999). For metabolic studies single mice were kept for 24-hours in metabolic cages (3600M021, Techniplast) and urine and stool production, as well as water and food intake were measured. Treatments were performed with dDAVP (0.4 μ g/kg intraperitoneally) or furosemide (40mg/kg intraperitoneally) and effects on these parameters were assessed. For all animal studies, institutional approval was granted and international guidelines for the care and use of laboratory research animals were followed. ARRIVE guidelines for reporting of animal studies were followed. Age and gender information of mice used in the experiments is provided in the Results and Figure Legends section.

METHOD DETAILS

Western blotting

Kidneys were lysed in NP40 lysis buffer (Life Technologies) with 1mM PMSF and protease inhibitor cocktail (Complete, Roche) using the QIAGEN TissueLyser-II. After centrifugation, the protein concentrations in the supernatant were determined with a Bradford assay. Equal amounts of protein were loaded onto NuPage 4%–12% Bis-Tris gels (Life Technologies) and blotted to nitrocellulose membranes. Equal protein loading was assessed using a rabbit polyclonal anti- β -actin antibody (Cell Signaling Technology Cat# 4970, RRID:AB_2223172). Antibodies against NKCC2 (Cell Signaling Technology, Cat# 38436, RRID:AB_2799134), NCC (Millipore Cat# AB3553, RRID:AB_571116) and TRPM6 (Thermo Fisher Scientific Cat#PA5-77326, RRID:AB_2736741) were used as well. HRP-conjugated secondary antibodies were used and chemiluminescence signal was determined with the SuperSignal WestPico chemiluminescent substrate (Pierce).

Immunolabeling of kidney sections and morphological kidney analyses

For morphological analysis of mouse kidneys, kidneys were fixed in 4% paraformaldehyde. Kidneys were bisected and then processed and embedded in paraffin for histological analysis. H&E stainings, lacZ stainings and TUNEL assays were performed according to standard protocols. The other kidney half was embedded in 30% sucrose and subsequently in OCT for immunolabeling experiments. For immunolabeling, 7 μ m kidney sections were permeabilized in 0.5% Triton X-100 and subsequently blocked with 5% serum in which the secondary antibodies were raised. The following primary antibodies were used: rabbit anti- β -galactosidase (Thermo Fisher Scientific Cat# A-11132, RRID:AB_221539), chicken anti- β -galactosidase (Abcam Cat# ab9361, RRID:AB_307210), goat anti-Aqp2 (Santa Cruz Biotechnology Cat# sc-9882, RRID:AB_2289903), rabbit anti-GFP (Thermo Fisher Scientific Cat# A-11122, RRID:AB_221569), rabbit anti-NKCC2 (Cell Signaling Technology, Cat# 38436, RRID:AB_2799134), goat anti-THP (Santa Cruz Biotechnology Cat# sc-19554,

RRID:AB_793728), rabbit anti-parvalbumin (Abcam Cat# ab11427, RRID:AB_298032), goat anti-EGF (R&D Systems Cat# AF2028, RRID:AB_355111), active β -catenin (non-phospho Ser33/37/Thr41) (Cell Signaling Technology Cat# 8814S, RRID:AB_11127203), anti-TRPV5 (MyBioSource Cat# MBS9125453), anti-Cldn14 (MyBioSource Cat# MBS1494658), and anti-Cldn19 (BiCell Scientific, Cat# 00219). Phalloidin conjugated with Alexa647 (Thermo Fisher Scientific Cat# A22287, RRID:AB_2620155) was used for cytoskeletal staining at a dilution of 1:100. DAPI was used to stain nuclei (Thermo Fisher Scientific Cat# D3571, RRID:AB_2307445). Secondary Alexa 488/555/647 antibodies were used at a dilution of 1:200 (Thermo Fisher). Controls included stainings with no primary antibody or with IgG control primary antibodies. Rhodamine-conjugated peanut agglutinin lectin (Vector Laboratories Cat# RL-1072, RRID:AB_2336642) [epithelial staining of distal nephron epithelial cells; contiguous staining of PTs] was used at a dilution of 1:100.

Semiquantitative RT-PCR

For gene expression studies, cDNA was obtained using the Transcriptor First strand synthesis kit utilizing hexamer primers (Roche). Semiquantitative RT-PCR was performed using a LightCycler 480 system with the LightCycler 480 SYBR Green I master mix according to standard procedures (45 amplification cycles) (Roche Applied Science, Indianapolis, IN). Primers for 36b4 were used as a normalization control. Concentrations were determined using a standard dilution curve. Experiments for all samples were performed in triplicate. Primer sequences for semiquantitative RT-PCR are listed in [Table S1](#).

ELISAs, serum and urine chemistries

Serum levels of 1,25 (OH)₂ vitamin D₃ were measured with an EIA kit by immunoextraction followed by quantitation with an enzyme-immunoassay (ImmunoDiagnosticSystems PLC, Tyne and Wear, UK; Cat# AC-62F1). Mouse serum FGF23 was measured using the Quidel ELISA Kit that measures C-terminal FGF-23 according to the manufacturer's instructions (Quidel, San Diego, USA; Cat# 60-6300). Mouse PTH serum levels were determined with an ELISA kit that measures intact PTH (PTH 1-84) (Quidel, San Diego, USA; Cat # 60-2305). Mouse serum chemistries were determined with a Dri-Chem7000 chemistry analyzer (Heska). Urine chemistries were determined with a Roche ModP analyzer. Ionized serum calcium measurements were performed with a Siemens RAPIDlab 348EX machine.

Bone analyses

Hindlimbs were dissected and fixed in Bouin's fixative for 2 weeks and subsequently processed for paraffin embedding, sectioned and stained by H&E according to standard protocols. A second group of hindlimbs were fixed in 4% paraformaldehyde for 2 days and subsequently processed and embedded in resin. These non-decalcified mineralized bones were used for Van Kossa stainings to visualize calcified bone or for Goldner-Trichrome stainings. Femurs from mice were subjected to bone histomorphometric analysis. Fixed bones were dehydrated in graded ethanol, then infiltrated and embedded in methylmethacrylate without demineralization. Undecalcified 5 mm and 10 mm thick longitudinal sections were obtained using a microtome (RM2255, Leica Biosystems., IL, USA). The 5 mm sections were stained with Goldner-Trichrome and at least two nonconsecutive sections per sample were examined for measurement of cellular parameters. A standard bone histomorphometric analysis of the femoral metaphysis was done using the Osteomeasure analyzing system (Osteometrics Inc., Decatur, GA, USA). Measurements were performed in the area of secondary spongiosa, 250-300 μ m below the proximal growth plate. The observer was blinded to the experimental genotype at the time of measurement. The structural and cellular parameters were calculated and expressed according to the standardized nomenclature ([Dempster et al., 2013](#)). For μ CT analysis of tibias and femurs, the bones were dissected from each animal and collected into individual glass vials with 4% paraformaldehyde. Samples were fixed overnight at 4°C on a shaker. After overnight fixation, samples were kept in paraformaldehyde solution to be assessed with μ CT. A Scanco Medical MicroCT 35 system with an isotropic voxel size of 7 μ m was used to image the samples. Scans were conducted with an X-ray tube potential of 70kVp, an X-ray intensity of 0.145 mA and an integration time of 600ms per tomographic projection. 3-Dimensional images were reconstructed and obtained from the scans. Whole body skeletal imaging was performed using a Siemens Inveon PET-CT.

QUANTIFICATION AND STATISTICAL ANALYSIS

RNA-seq data analysis

Analysis of RNA-seq data was performed based on datasets that we recently reported: (1) P8 Six2Cre⁺KCTD1^{fl/fl} mice and littermate KCTD1^{fl/fl} control mice (n = 4 per group); (2) 4-months-old β -actinCreERT2⁺TFAP2B^{fl/fl} mice versus control littermates treated with TAM at 6 weeks of age (n = 4 per group) ([Marneros, 2020](#)). RNA-seq data has been deposited to the GEO database: GSE126326 and GSE130864.

Statistics

An unpaired two-tailed Student's t test was used for statistical analyses. P values < 0.05 were considered to be statistically significant. P values are indicated. Graphs show mean \pm SEM. Graphs, heatmaps and analyses were performed with GraphPad Prism version 8.4.3.

Cell Reports, Volume 34

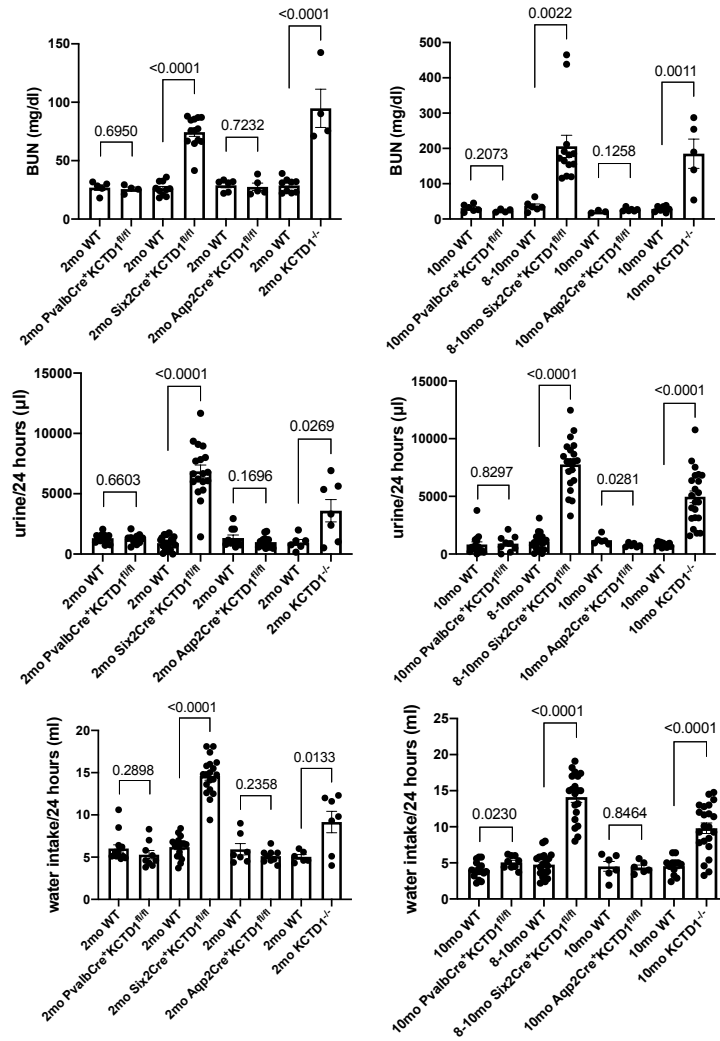
Supplemental Information

Magnesium and Calcium Homeostasis

Depend on KCTD1 Function in the Distal Nephron

Alexander G. Marneros

A



B

		Na	K	Cl	Na/K ratio	BUN	Cre	Ca	phosphorous	Mg	albumin	TP
control	2mo (n=5)	150.60	7.70	107.40	19.60	26.94	0.28	11.46	9.88	2.80	2.48	5.08
PvalbCre ⁺ KCTD1 ^{fl/fl}	2mo (n=4)	151.50	8.00	108.50	19.25	25.68	0.23	11.40	9.58	2.28	2.45	5.00
ttest control vs KO		0.12687037	0.49325971	0.42469636	0.75408365	0.69502674	0.28740834	0.72943431	0.51613975	0.00039824	0.68452834	0.52988373
control	2mo (n=8)	150.13	7.85	109.13	19.63	26.50	0.26	11.34	9.94	2.79	2.63	5.24
PvalbCre ⁺ TFAP2B ^{fl/fl}	2mo (n=4)	148.25	8.05	111.25	18.75	27.20	0.20	10.80	7.90	1.95	3.23	5.90
ttest control vs KO		0.14552826	0.77233899	0.19893743	0.64878761	0.79469171	0.13213259	0.27678437	0.02197912	0.00318728	0.03807475	0.07375455
control	10mo (n=6)	151.00	10.30	114.33	15.00	31.02	0.24	12.12	10.07	3.32	2.65	5.68
PvalbCre ⁺ KCTD1 ^{fl/fl}	10mo (n=4)	152.25	8.45	112.25	18.25	23.63	0.23	11.03	7.43	2.48	2.73	5.58
ttest control vs KO		0.41584649	0.0463292	0.18731496	0.02898833	0.20731261	0.24150397	0.07387967	0.04569195	0.00031776	0.48604202	0.39248571
control	10mo (n=6)	151.00	10.30	114.33	15.00	31.02	0.23	12.12	10.07	3.32	2.65	5.68
PvalbCre ⁺ TFAP2B ^{fl/fl}	10mo (n=3)	151.00	7.77	111.00	19.67	33.30	0.20	12.57	9.00	2.83	2.93	5.77
ttest control vs KO		1	0.02525945	0.08056513	0.01384075	0.7152906	0.31589066	0.50825974	0.43909094	0.02624803	0.05904942	0.61690303

Figure S1: Kidney function in PvalbCre+KCTD1^{fl/fl} mice.

- (A) Measurements of BUN serum levels (in mg/dl), 24-hour urine production and 24-hour water intake in 2-month-old and 10-month-old groups of PvalbCre+KCTD1^{fl/fl} mice, Six2Cre+KCTD1^{fl/fl} mice, Aqp2Cre+KCTD1^{fl/fl} mice, KCTD1^{-/-} mice and their respective WT controls.
- (B) Serum chemistries in 2-month-old and 10-month-old groups of PvalbCre+KCTD1^{fl/fl} mice, PvalbCre+TFAP2B^{fl/fl} mice and their control littermates. BUN, creatinine, magnesium, phosphorus and total calcium in mg/dl. Chloride, potassium and sodium in mEq/l. Albumin and total protein in g/dl.

Related to Figure 1.

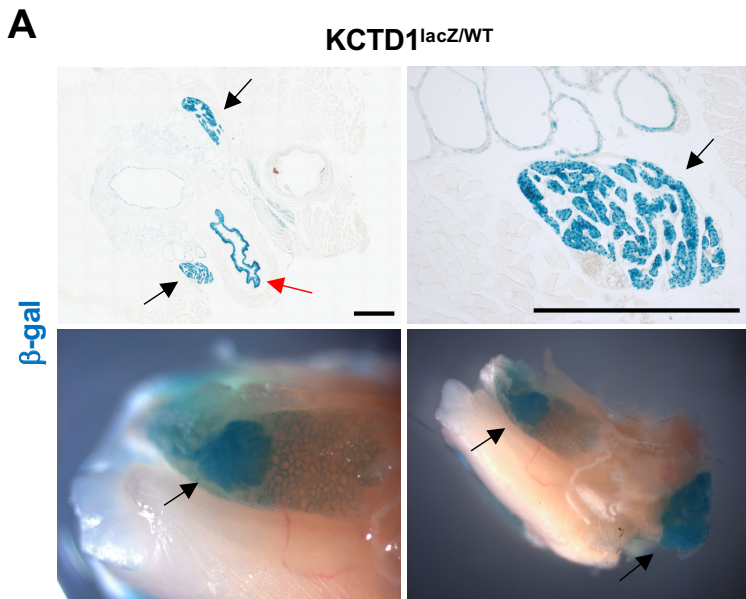
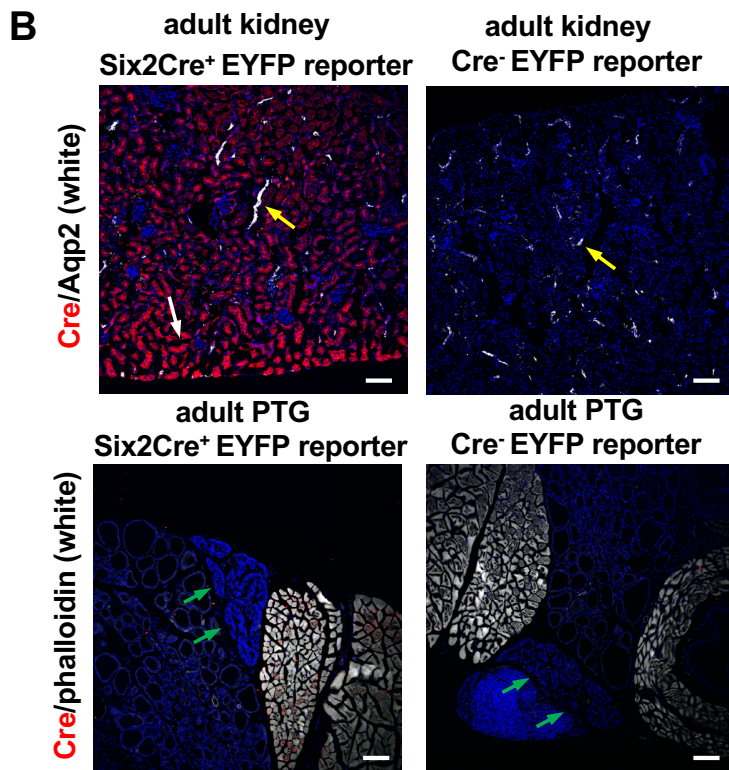


Figure S2: KCTD1 is expressed in PTGs and Six2Cre⁺ mice show Cre activity in the nephron epithelium except the CDs but no activity in PTGs that are targeted by PTHCre⁺ mice.

(A) Staining for β-galactosidase in KCTD1^{lacZ/WT} mice shows that KCTD1 is strongly expressed in PTGs (black arrows). The epithelium of the esophagus shows KCTD1 expression as well (red arrow). Scale bars, 500μm.

(B) Top: Adult Six2Cre⁺ROSA26Sor^{tm3(CAG-EYFP)} (Ai3) reporter mice show strong Cre activity (red, GFP immunolabeling) in the nephron (white arrow) except the CDs (Aqp2, white; yellow arrow). Bottom: No Cre activity is observed in the PTGs (green arrows) of these mice. Scale bars, 100μm.

(C) Adult PTHCre⁺ROSA26Sor^{tm3(CAG-EYFP)} (Ai3) reporter mice show strong Cre activity in the PTGs (green). Scale bar, 500μm.



Related to Figure 3.

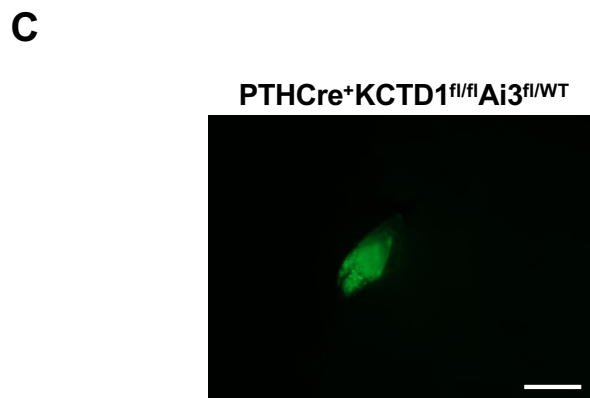


Figure S2

Primer Name	Primer Sequence (5' to 3') UP	Primer Sequence (5' to 3') DW
mouse primers		
36b4	TCACTGTGCCAGCTCAGAAC	AA TTTCAA TGGTGCCTCTGG
Trpv6	GTCATGTACTTTGCCAGAGGA	TATAGAAGGCTGAAGCAAATCCCA
Trpv5	GAAACTTCTCAATTGGTGGGTCAG	TTTGCCGGAAGTCACAGTT
Clcnkb	GTGGGTCCTTTTTACAACGC	CTGGAGCAAGTGATCCAAGTC
Pth1rvar2	CAGGCGCAATGTGACAAGC	TTCCCGGTGCCTTCTCTTTC
Kcnj1 (ROMK)	CATCCTTTCTGTCAGTGCCC	GAACAGCACCCTCACTTG
Atp1a1	GGGGTTGGACGAGACAAGTAT	CGGCTCAAATCTGTTCCGTAT
Claudin-19	TCCTCTTGGCAGGTCTCTGT	GTGCAGCAGAGAAAGGAACC
Claudin-16	CAAACGCTTTTGATGGGATTC	TTTGTGGGTCATCAGGTAGG
Slc34a3	AGACAGGCACCAGGTACCAC	CAGCCCTGCAGACATGTTAAT
Slc34a1	TTGTCAGCATGGTCTCCTCC	CAAAAGCCCGCCTGAAGTC
Claudin-14	ACCCTGCTCTGCTTATCC	GCACGGTTGTCCTTGTAG
NKCC2 (Slc12a1)	ATGCCTCGTATGCCAAATCT	CCCACATGTTGTAATCCATA
TRPM6	CCTTGGGGAGTCATTGAGAAC	CAGTCCCATCATCACACAGG
NCX1	TGAGAGGGACCAAGATGATGAGGAA	TGACCCAAGACAAGCAATTGAAGAA
calbindin D28K	ACTCTCAAACCTAGCCGCTGCA	TCAGCGTCGAAATGAAGCC

Table S1: Primers used for semiquantitative RT-PCR.

Related to STAR methods.